cmgh
CELLULAR AND MOLECULAR GASTROENTEROLOGY AND HEPATOLOGY

ORIGINAL RESEARCH

TRPV6-mediated Store-operated Ca^{2+} Entry Participates in Pancreatic Acinar Cell Injury During Acute Pancreatitis

Chenxia Han,[1,*] Yuncheng Luo,[2,*] Zhenlu Li,[1] Lu Li,[1] Jiawang Li,[1] Ping Liao,[2] Li Li,[3] Juan Lin,[4] Shiyu Liu,[1] Tingting Liu,[1] Dan Du,[1,5] Wei Huang,[1,6] Ruotian Jiang,[2] and Qing Xia[1]

[1]West China Centre of Excellence for Pancreatitis, Institute of Integrated Traditional Chinese and Western Medicine, West China Hospital, Sichuan University, Chengdu, China; [2]Laboratory of Anesthesia and Critical Care Medicine, National-Local Joint Engineering Research Center of Translational Medicine of Anesthesiology, West China Hospital, Sichuan University, Chengdu, China; [3]Institute of Clinical Pathology, West China Hospital, Sichuan University, Chengdu, China; [4]Liverpool Pancreatitis Research Group, Institute of Systems, Molecular and Integrative Biology, University of Liverpool, Liverpool, United Kingdom; [5]Advanced Mass Spectrometry Center, Research Core Facility, Frontiers Science Center for Disease-related Molecular Network, West China Hospital, Sichuan University, Chengdu, China; and [6]West China Biobank, West China Hospital, Sichuan University, Chengdu, China

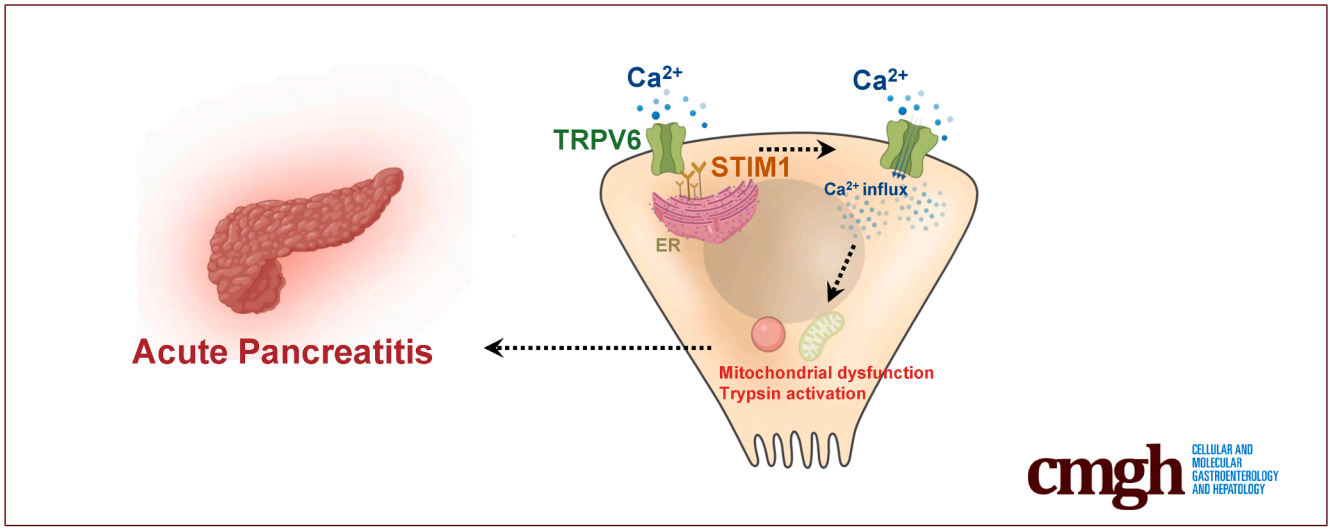

SUMMARY

Transient receptor potential vanilloid 6 (TRPV6) expression is increased in mice and patients with acute pancreatitis, as well as it-mediated store-operated Ca^{2+} entry signals, which rely on the physical interaction between TRPV6 and stromal interaction molecule 1. Inhibiting TRPV6 has a protective effect against experimental acute pancreatitis.

BACKGROUND & AIMS: Suppressing toxic Ca^{2+} accumulation in pancreatic acinar cells (PACs) is the central therapeutic strategy of acute pancreatitis (AP). Store-operated Ca^{2+} entry (SOCE) represents an important mechanism promoting Ca^{2+} overload, which remains incompletely understood in AP. Transient receptor potential vanilloid 6 (TRPV6) is an ion channel highly selective to Ca^{2+}, and its role in PACs or AP onset remains largely unknown.

METHODS: We utilized human and mouse pancreata for TRPV6 expression using RNAscope and PACs for electrophysical currents and Ca^{2+} signals identification. Following RNA sequencing, we examined the interaction between TRPV6 and stromal interaction molecule 1 (STIM1) at the junctions between the endoplasmic reticulum (ER) membrane and the plasma membrane using coimmunoprecipitation, living cell imaging, and transmission electron microscopy. Finally, we established a mouse model using adeno virus-mediated pancreas conditional *Trpv6* knockdown. We thereafter utilized a TRPV6 inhibitor to examine the effect of inhibiting TRPV6 on AP.

RESULTS: The in situ TRPV6 expression and cation currents were significantly enhanced in PACs during AP. Pancreatic genetic conditional knockdown and pharmacological blockade of TRPV6 both showed beneficial effect on AP mice, which may be attributed to the prevention of mitochondrial depolarization and trypsin activation in PACs. Additionally, TRPV6 was found to participate in ER store-deletion-induced Ca^{2+} signals in mouse and human PACs, and to interact with STIM1, implicating its involvement in mediating SOCE that contributes to AP pathology.

CONCLUSIONS: TRPV6 is a key player in Ca^{2+} overload in PACs and contributes to AP at least partly through mediating

SOCE. *(Cell Mol Gastroenterol Hepatol 2025;19:101620; https://doi.org/10.1016/j.jcmgh.2025.101620)*

Keywords: Acute Pancreatitis; TRPV6; Store-operated Ca^{2+} entry; STIM1.

Acute pancreatitis (AP) is a common digestive disease characterized by sterile pancreatic inflammation.[1] Clinical cases of severe AP have a 35% mortality rate, mainly due to multiple organ failure.[2] Ca^{2+} is essential for stimulating pancreatic excretion. However, excessive Ca^{2+} loading within pancreatic acinar cells (PACs) triggers mitochondrial dysfunction and the activation of trypsin, resulting in cell death and tissue injury.[3,4] Although the pathological mechanism of AP has not yet been targeted therapeutically,[5] the prevention of toxic intracellular Ca^{2+} accumulation appears to be a promising treatment for AP.[6,7] Multiple cellular stress signaling mechanisms, including mitochondrial depolarization, trypsin activation, and endoplasmic reticulum (ER) stress, have been shown to participate in PACs injury, and most of them are related to excessive intracellular Ca^{2+} accumulation in PACs, a key feature of AP pathology.[8,9]

Store-operated Ca^{2+} entry (SOCE) has emerged as an essential pathway promoting excessive Ca^{2+} loading during AP.[8–10] In PACs, SOCE functions to replenish intracellular Ca^{2+} levels required to support essential pancreatic excretion. However, SOCE hyperactivity results in excess Ca^{2+} and cell death. It was shown that restoring negative regulation of SOCE, resulting in SOCE suppression, could protect against AP.[10] The Ca^{2+}-sensitive receptor stromal interaction molecule 1 (STIM1) is localized to the ER and functions as a primary mediator of SOCE[11] through physical interactions with different SOCE channels, such as Orai1.[12] However, this mechanism remains incompletely understood due to the uncertain location of STIM1-Ca^{2+} channel interactions, as well as the nature of Ca^{2+} entry channels in PACs.

The highly selective Ca^{2+} channel transient receptor potential vanilloid 6 (TRPV6, also known as ECaC2 or CaT1), is a member of the TRP vanilloid subfamily,[13] a group of cation channels that have been discovered to participate in various inflammatory conditions in humans.[14] TRP subfamily members including vanilloid (TRPV1,[15–24] TRPV4[25,26]), ankyrin (TRPA1),[24,25,27,28] canonical (TRPC3,[29,30] TRPC6[30]), and melastatin (TRPM2[31]) have already been reported to be associated with AP. TRPV6 has been previously reported to play a role in chronic pancreatitis,[32], hereditary pancreatitis,[33] and pancreatic cancer.[34] However, the role of TRPV6 in AP and how it functions or participates in the disease pathology remains unclear, restricting its potential as a therapeutic target in AP treatment.

Although TRPV6 is broadly recognized as a Ca^{2+} entry channel, the designation of SOCE for TRPV6 remains contentious. Earlier research claimed that TRPV6 could mediate SOCE in Chinese hamster ovary-K1 cells,[35] lymphocytes,[36] and prostate cancer epithelial cells,[37] whereas other researchers reached the opposite conclusion in human lymph node prostate cancer cells.[38] In recent years, TRPV6 inhibition was shown to reduce Ca^{2+} influx into cells following depletion of ER Ca^{2+} storage in prostate cancer cells.[39] Significant decrease in ER-clearance-induced Ca^{2+} entry signal after TRPV6 inhibition, which supports the involvement of TRPV6 in SOCE ,[40] and a recent study also revealed that TRPV6 participate in SOCE in human lymph node prostate cancer cells.[41] A comprehensive understanding is that TRPV6 at least has a modulatory or auxiliary role in SOCE influx under certain conditions.[42] Notably, this mechanism has not been tested in PACs during AP; as the primary role of Ca^{2+} in AP pathology, it is worthy to reveal the role of TRPV6-mediated Ca^{2+} in AP and seek a possible therapeutic path.

Here, we examined TRPV6 functional expressions in PACs using in situ RNAscope as well as whole-cell patch clamp recordings in mouse and human PACs. Then, to determine the function of TRPV6 in AP pathology and elucidate the cellular mechanisms mediating Ca^{2+} influx, we investigated the SOCE mechanism mediated by TRPV6 in both mouse and human PACs and performed adeno-associated virus (AAV)-mediated pancreatic *Trpv6* knockdown in AP mice. Our data reveal TRPV6 as a novel component of SOCE, an initial mechanism leading to Ca^{2+} overloading during AP.

Results

Functional Expression of TRPV6 in Mouse and Human PACs

Previous studies have preliminarily reported the expression of TRPV6 in pancreas.[43–46] Here, using RNAscope, we examined *Trpv6* expression under pathological and physiological conditions in the pancreata of mice

***Authors share co-first authorship.**

Abbreviations used in this paper: **AAV, adeno-associated virus; ANOVA, analysis of variance; AP, acute pancreatitis; BP, biological process; BSA, bovine serum albumin; CC, cell component; CCK, cholecystokinin; CER, cerulein; Co-IP, coimmunoprecipitation; DAPI, 4',6-diamidino-2-phenylindole; DEGs, differently expressed genes; DMEM, Dulbecco's modified Eagle medium; DNB, DNA nanoball; DVF, divalent-free; EM, ER membrane; ER, endoplasmic reticulum; FBS, fetal bovine serum; GSEA, Gene Set Enrichment Analysis; GO, Gene Ontology; H&E, hematoxylin and eosin; HEK, human embryonic kidney; HRP, horseradish peroxidase; IF, immunofluorescence; IHC, immunohistochemistry; IP_3, inositol triphosphate; KEGG, Kyoto Encyclopedia of Genes and Genomes; MF, molecular function; MPO, myeloperoxidase; NC, negative control; PACs, pancreatic acinar cells; PBS, phosphate buffered saline; PI, propidium iodide; PM, plasma membrane; RNA-seq, RNA, sequencing; RT-qPCR, reverse transcription-quantitative polymerase chain reaction; SEM, standard error of the mean; SERCA, sarco(endo)plasmic reticulum calcium ATPase; SOCE, store-operated Ca2+ entry; SP, substance P; STIM1, stromal interaction molecule 1; TG, thapsigargin; TLCS, taurolithocholic acid 3-sulfate disodium salt; TMRM, tetramethylrhodamine; TRP, transient receptor potential; TRPV6, transient receptor potential vanilloid 6; VFF, von Frey filaments.**

Most current article

2352-345X
https://doi.org/10.1016/j.jcmgh.2025.101620

treated with cerulein (CER) to induce AP (AP mice) and control mice treated with phosphate buffered saline (PBS). PACs compose the basic functional unit of the exocrine pancreas and play central roles in AP,[47] so we labeled PACs using a primary antibody against amylase. As the data show, the proportion of TRPV6-positive PACs was significantly increased in AP mice compared with controls (Figure 1*A*). Similarly, AP mice showed considerably higher levels of pancreatic TRPV6 protein than the control group (Figure 1*B*). Next, we examined TRPV6 expression in

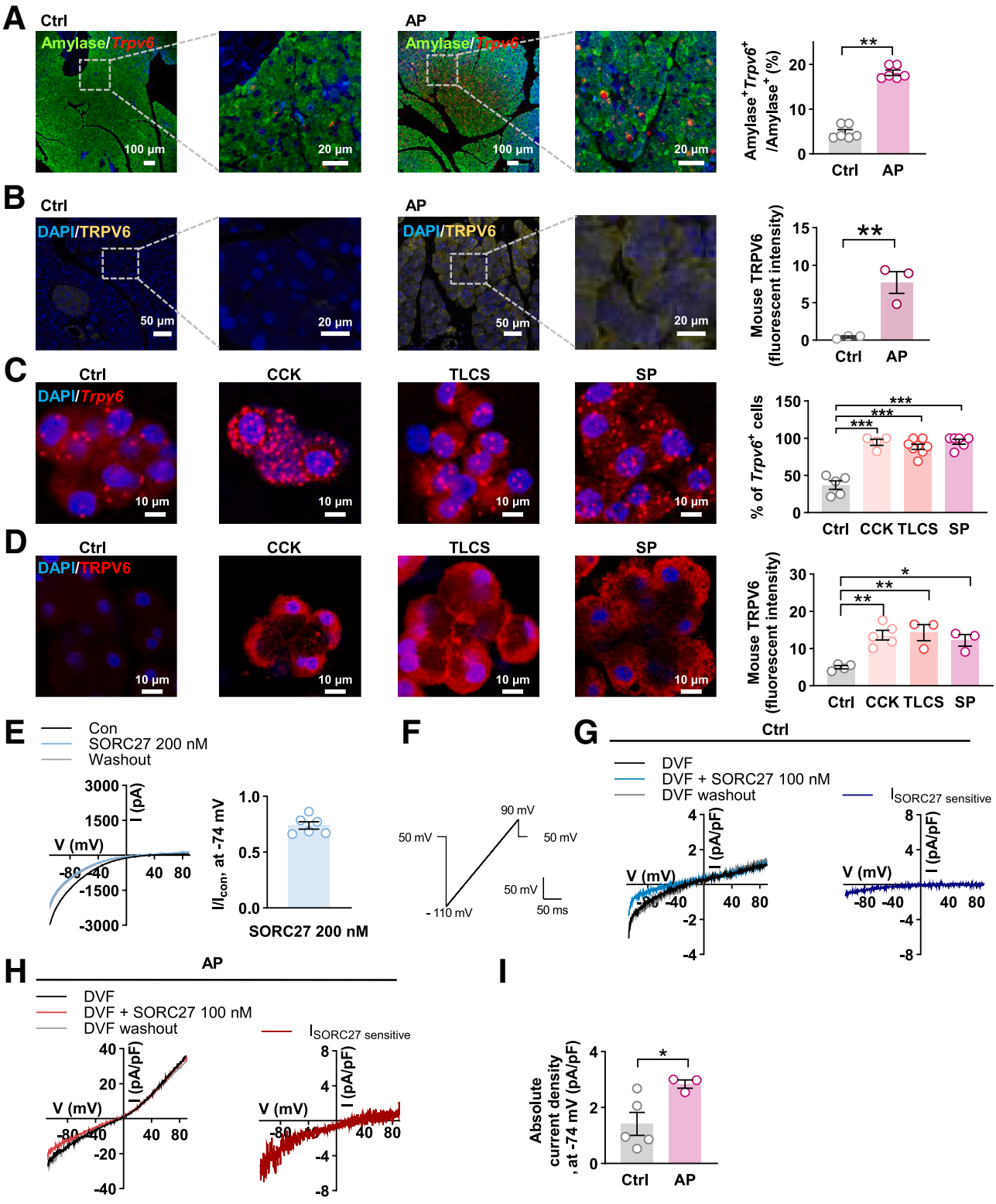

freshly isolated mouse PACs treated with different toxins, including cholecystokinin (CCK),[48] taurolithocholic acid 3-sulfate disodium salt (TLCS),[49] and substance P (SP).[50] Compared with control PACs, the proportion of cells expressing *Trpv6* was significantly increased following treatment with any of the toxins (Figure 1*C*). TRPV6 antibody labeling of PACs further demonstrated significantly increased TRPV6 protein expression that was mostly localized to cell membranes following each of the treatments (Figure 1*D*). We next examined TRPV6-mediated currents in freshly isolated PACs using patch-clamp electrophysiology. SORC27, a TRPV6 inhibitor, was previously shown to reduce TRPV6-mediated current amplitude by 34% in human embryonic kidney (HEK)-293T cells overexpressing *TRPV6*,[51] which was confirmed experimentally in our data (~26%) (Figure 1*E*). Next, whole-cell patch clamp recordings with a 200-ms linear voltage ramp ranging from −110 mV to +90 mV (Figure 1*F*) were performed on freshly isolated PACs from both control and AP mice, using extra- and intracellular solutions optimized for measuring TRPV6-mediated cation currents.[52] As shown in Figure 1*G and H*, the currents were reduced by 100 nM SORC27 in both control and AP PACs. Subtracting the SORC27-sensitive current from the total current revealed an inward rectifying current exhibiting voltage-dependent gating, similar to previous descriptions of TRPV6-mediated currents.[53] In agreement with the elevated TRPV6 expression observed in AP mice, SORC27-sensitive currents were upregulated in AP PACs (Figure 1*I*), indicating enhanced TRPV6 channel activity.

To extend these results to humans, clinical human pancreatic specimens were collected and used to prepare tissue sections and isolate PACs (Figure 2*A*). Although it is not feasible to obtain human pancreatic tissue during initial AP, we have collected pancreas tissues that adjacent to the necrotized tissues from patients who met the criteria for surgical intervention of severe AP and subsequently underwent pancreatic necrosectomy. Normal pancreatic tissues from patients who underwent surgery for left-sided or small unobstructing pancreatic tumors were used as controls. Consistent with observations from the AP mice model, *TRPV6* gene expression in PACs was significantly elevated in pancreata of AP surgery patients compared with controls (Figure 2*B*). Freshly isolated human PACs were then analyzed using the whole-cell patch clamp technique. SORC27-sensitive currents recorded from human PACs of AP patients exhibited similar characteristics to those recorded in mice (Figure 2*C*). Collectively, these data reveal that TRPV6 is functionally expressed both in both mouse and human PACs and upregulated during AP.

TRPV6-mediated Ca^{2+} Influx in Mouse and Human PACs

TRPV6 is highly permeable to Ca^{2+}, an important ion mediator for pancreatic exocrine function,[3,4] and Ca^{2+} overload is a primary mechanism of cell injury during AP onset.[8,54] Blocking TRPV6 with SORC27 reduced Ca^{2+} influx following exposure to toxins in freshly isolated PACs from mice (Figure 3*A–B*) and humans (Figure 3*C–D*). To validate the pharmacological results, we generated mice with pancreatic *Trpv6* knockdown achieved by AAV-mediated transduction of the pancreas through pancreatic duct infusion (Figure 3*E*) according to a previous protocol,[55] referred to as si*Trpv6*, and a control AAV construct is referred to as siNC. We confirmed knockdown efficiency on pancreatic *Trpv6* in PACs using fluorescent imaging (AAV was labeled by green fluorescent protein) and reverse transcription-quantitative polymerase chain reaction (RT-qPCR) (Figure 3*F*), revealing an approximate 81% reduction in *Trpv6* mRNA levels. As shown in Figure 3*G*, PACs from si*Trpv6* mice showed significantly reduced Ca^{2+} influx following CCK exposure compared with siNC PACs. This result suggests that TRPV6 could mediate Ca^{2+} influx in mouse PACs, which might contribute to further cell injury related to Ca^{2+} overload.

Next, we examined whether pancreatic *Trpv6* knockdown could protect PACs from cell injury. As expected, PACs isolated from si*Trpv6* mice had increased cell viability following CCK and TLCS stimulation compared with siNC PACs (Figure 3*H*). Trypsin activation and mitochondrial dysfunction are two fundamental cellular pathological mechanisms observed during AP.[3] We examined mitochondrial dysfunction in PACs using a cell-permeable voltage-sensitive fluorescent dye, TMRM, which loses fluorescence following pathological mitochondrial depolarization. Live-cell imaging revealed that CCK-induced mitochondrial depolarization was significantly reduced in si*Trpv6* PACs compared with siNC (Figure 3*I*). Meanwhile, we visualized PAC trypsinogen activation in real time using a trypsin-sensitive fluorescent probe, BZiPAR, revealing that CCK-mediated trypsin activation was significantly inhibited in si*Trpv6* compared with siNC PACs (Figure 3*J*).

Figure 1. (***See previous page***). **Increased TRPV6 expression and current in mouse PACs.** (*A*) Representative images and quantification of pancreatic *Tprv6* gene expression in AP and control (Ctrl) mice (n = 6 sections from 3 mice per group). (*B*) Representative images and quantification of TRPV6 protein expression in ctrl and AP mouse pancreas tissue (n = 3 sections from 3 mice per group). (*C*) Representative images and quantification of *Tprv6* expression in freshly isolated PACs from AP and Ctrl mice (n = 4 – 8 samples from 3 mice per group). (*D*) Representative images and quantification of TRPV6 protein expression in untreated control PACs and following treatment with the indicated toxics (n = 3–5 samples from 3 mice per group). (*E*) Typical whole-cell current traces and quantification of the effect of SORC27 (200 nM) on inward currents in HEK293T cells (n = 6 cells from 3 independent experiments). (*F*) Protocol for whole-cell patch clamp recordings with a 200-ms linear voltage ramp ranging from −110 mV to +90 mV on mouse PACs. (*G and H*) Typical whole-cell current traces showing the effect of SORC27 (100 nM) on inward currents (*left*) and SORC27-sensitive currents (*right*) in PACs from Ctrl (*G*) and AP (*H*) mice. (*I*) Quantification of current densities observed at –74 mV from Ctrl and AP PACs (n = 3–5 cells from 6 independent experiments per treatment). Data are the mean ± SEM; **P* < .05, ***P* < .01, ****P* < .001.

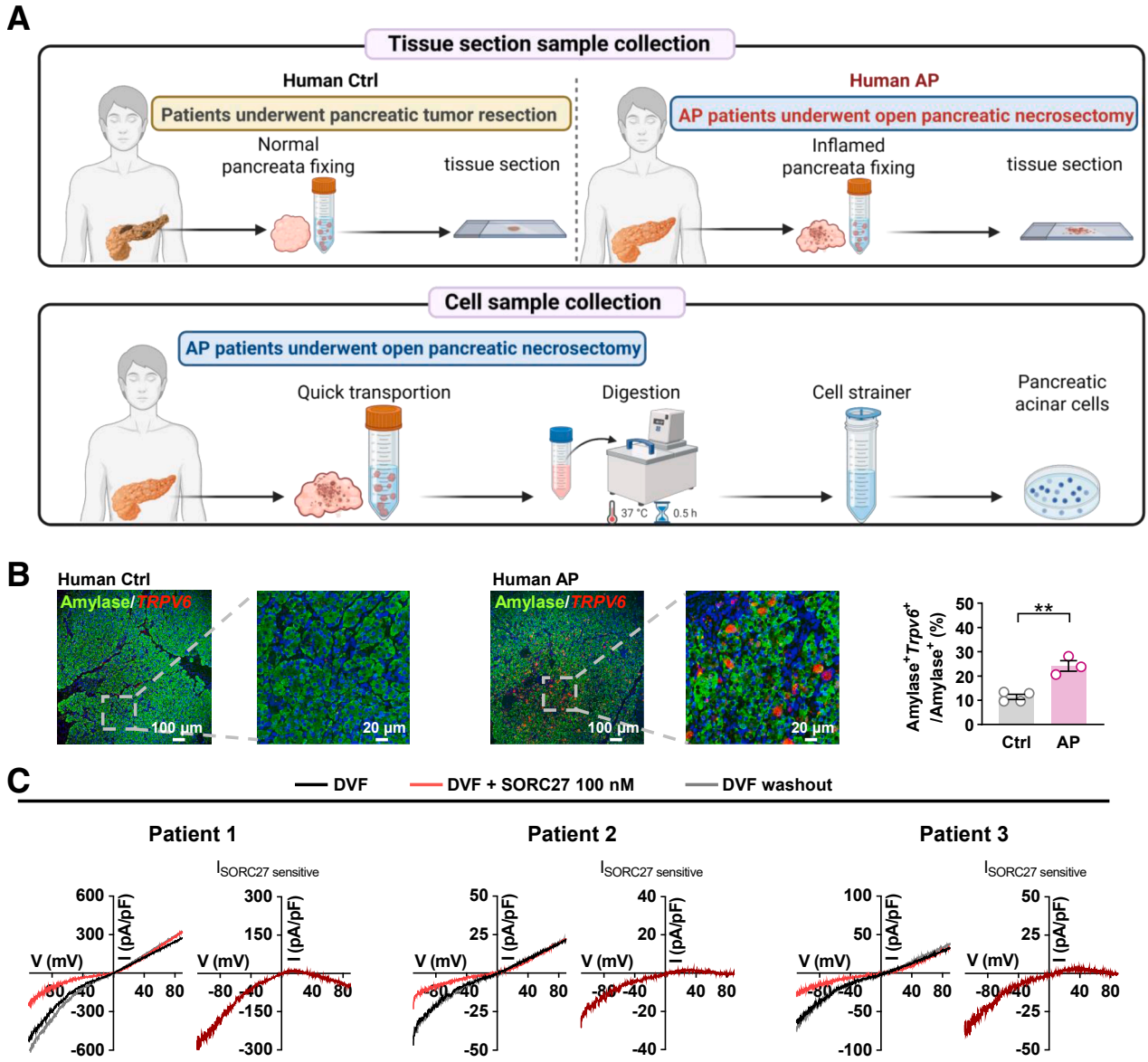

Figure 2. Elevated functional expression of TRPV6 in human PACs. (*A*) Schematic illustrating the approach for human sample collection. (*B*) Representative images and quantification of human pancreatic *TRPV6* gene levels (n = 4, 3 sections from 3 patients per group). (*C*) Typical whole-cell current traces showing the effect of SORC27 (100 nM) on inward currents (*left*) and SORC27-sensitive currents (*right*) in PACs from patients with AP (n = 3 cells from 3 patients with AP). Data are the mean ± SEM; $^{**}P < .01$.

These data demonstrate that *Trpv6* knockdown protected cell death, rescued mitochondrial depolarization, and inhibited trypsin activation.

TRPV6 Participates in SOCE by Interacting With STIM1

To define the mechanism underlying TRPV6-mediated PACs injury, we assessed transcriptome-wide variation in CCK-stimulated mouse PACs in the presence (CSOR) or absence (control) of SORC27 treatment (Figure 4*A*). In total, 2250 significant differentially expressed genes (DEGs) were identified ($Log_2|$fold change$| > 0.25$; adjusted $P < .05$). Kyoto Encyclopedia of Genes and Genomes (KEGG) pathway enrichment analysis of the DEGs revealed altered regulation of protein processing in ER (Figure 4*B*). Consistently, Gene Ontology (GO) enrichment terms relating to biological process (BP), cell component (CC), and molecular function (MF) also implicated ER function as being affected by TRPV6 (Figure 4*C*), with terms such as protein binding in ER, ER protein targeting, ER lumen and membrane, and ER signal peptide binding, among others, being differentially represented in SORC27-treated vs SORC27-untreated groups. Further, Gene Set Enrichment Analysis (GSEA) was performed to profile transcriptional differences between the groups, which revealed negative enrichment for ER and Ca^{2+}-related genes in the SORC27-treated compared

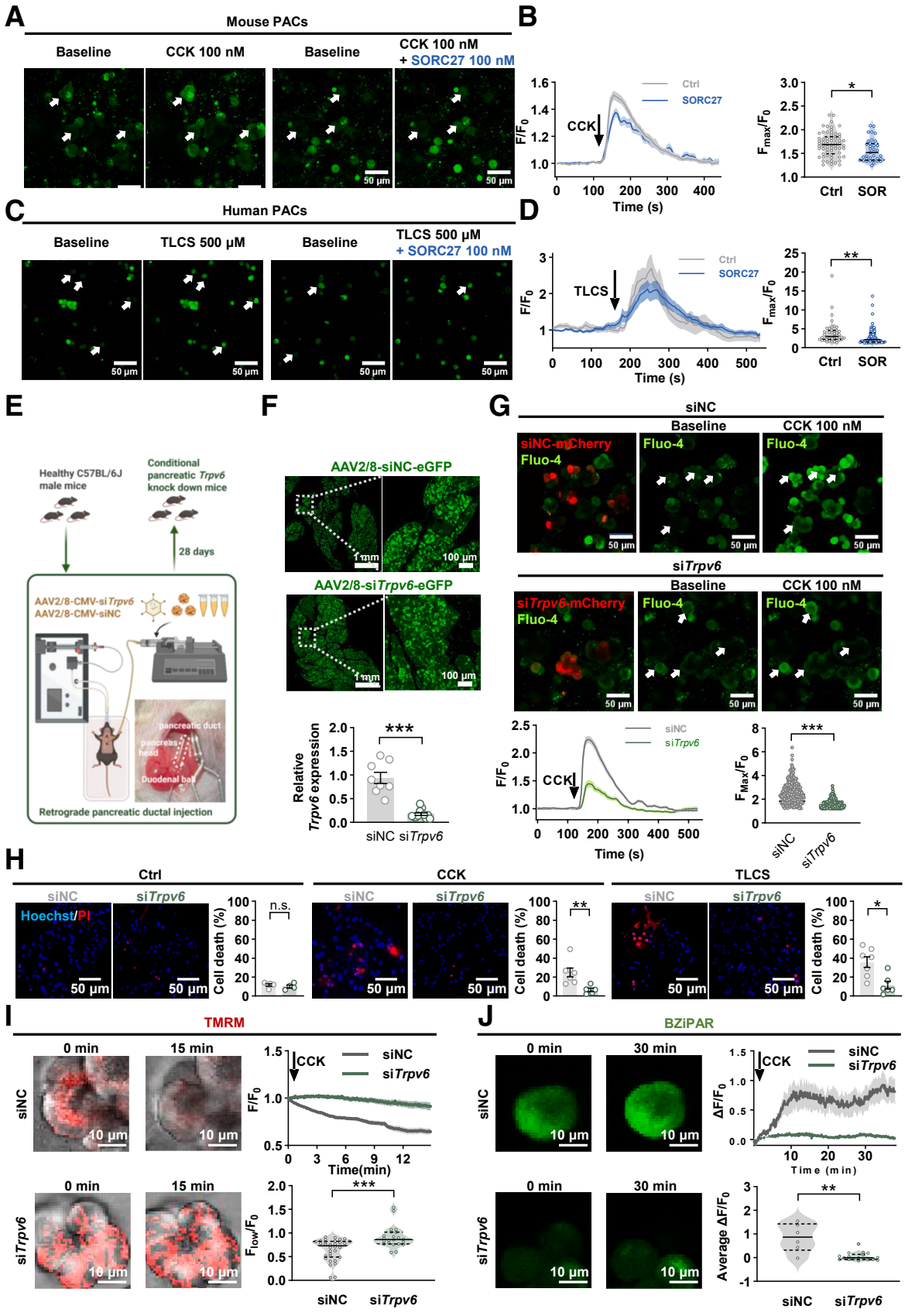
A
Mouse PACs
Baseline
CCK 100 nM
Baseline
CCK 100 nM
+ SORC27 100 nM
50 μm
B
Ctrl
SORC27
CCK
F/F0
Time (s)
Fmax/F0
Ctrl
SOR
C
Human PACs
Baseline
TLCS 500 μM
Baseline
TLCS 500 μM
+ SORC27 100 nM
D
TLCS
E
Healthy C57BL/6J male mice
Conditional pancreatic Trpv6 knock down mice
28 days
AAV2/8-CMV-siTrpv6
AAV2/8-CMV-siNC
pancreatic duct
pancreas head
Duodenal ball
Retrograde pancreatic ductal injection
F
AAV2/8-siNC-eGFP
1 mm
100 μm
AAV2/8-siTrpv6-eGFP
Relative Trpv6 expression
siNC siTrpv6
G
siNC
Baseline
CCK 100 nM
siNC-mCherry
Fluo-4
siTrpv6
siTrpv6-mCherry
H
Ctrl
CCK
TLCS
siNC
siTrpv6
Hoechst/PI
Cell death (%)
n.s.
I
TMRM
0 min
15 min
Time(min)
J
BZiPAR
0 min
30 min
ΔF/F0
Time (min)
Average ΔF/F0

with the SORC27-untreated group (Figure 4*D*), including genes encoding integral components of the luminal ER membrane, as well as genes associated with cellular responses to Ca^{2+}. These results suggest a close relationship between ER-mediated Ca^{2+} and TRPV6.

The polarized structure of PACs allows for secretory function, which is largely mediated by Ca^{2+} signaling.[8] The ER functions as a primary Ca^{2+} store and can release Ca^{2+} to support the physiological functions of PACs. The ER (or sarcoendoplasmic reticulum) ATPase (SERCA) transports Ca^{2+} into the ER, while the SERCA blocker thapsigargin (TG) inhibits ER Ca^{2+} filling, thus activating SOCE through the creation of a junction between ER membrane (EM) and plasma membrane (PM), known as the EM-PM junction.[56] The receptor-evoked Ca^{2+} signaling cascade is initiated by the release of ER Ca^{2+}, resulting in SOCE activation and subsequent refilling of the ER. Consequently, the EM-PM junction is the central structural component of SOCE.[57,58] Here, we analyzed the EM-PM junction by measuring the ER tracker (red fluorescence) signal that was in proximity to the PM signal labeled by cell mask (green fluorescence) in living PACs. As suggested, treatment with SORC27 significantly reduced the ER-PM signal following TG treatment (Figure 4*E*). We next confirmed this observation using transmission electron microscopy to examine the distance from EM to PM on freshly isolated mouse PACs, which showed that, after TG stimulation, the EM was in closer proximity to the PM in the basal PAC region compared with control PACs, and the EM-PM distance was significantly reduced by SORC27 treatment (Figure 4*F*).

The depletion of ER Ca^{2+} stores triggers SOCE, serving as an initial mechanism promoting Ca^{2+} overload. SOCE is mediated by a series of Ca^{2+}-sensitive elements, including diacylglycerol, inositol triphosphate (IP_3), and the Ca^{2+}-sensitive receptor STIM1 located in the ER.[11] To examine whether TRPV6-mediated Ca^{2+} signal participates in ER-induced Ca^{2+} replenishment, mouse PACs were placed in a Ca^{2+}-free extracellular fluid containing TG. TG induced a Ca^{2+} peak in the absence of extracellular Ca^{2+}, revealing ER Ca^{2+} depletion. With the addition of 2 mM Ca^{2+} to the extracellular fluid, Ca^{2+} influx was induced, representing SOCE-evoked Ca^{2+} influx induced by ER Ca^{2+} depletion (Figure 4*G*). SORC27 treatment significantly decreased the observed Ca^{2+} influx. Similar results were observed in human PACs (Figure 4*H*), revealing TRPV6 participation in TG-induced SOCE activation in both mouse and human PACs. Additionally, we have examined the effect of SORC27 on CCK-induced ER depletion and SOCE Ca^{2+} signal. As expected, TRPV6 significantly reduced SOCE activity without affecting ER Ca^{2+} releasing (Figure 4*I–K*).

As the ER Ca^{2+} sensor, STIM1 molecules cluster at the EM-PM membrane contact sites, subsequently activating the SOCE process to refill the ER Ca^{2+} storage.[11,59] Although IP_3 receptors have been suggested in SOCE activation, research claimed that the molecule responsible in PACs for sensing the ER Ca^{2+} concentration is more likely to be STIM1,[60] and STIM1 also responds as the first line to ER Ca^{2+} deletion and SOCE formation in PACs.[57] To further examine the role of TRPV6 in SOCE, we studied its interaction with STIM1. As shown in Figure 5*A–B*, STIM1 protein levels were elevated in both mice and human AP pancreata compared with their respective control groups; this observation is consistent with a previous study showing *Stim1* mRNA levels are increased in mouse PACs following carbachol stimulation.[10] To determine the interaction between TRPV6 and STIM1 in PACs, we performed structured illumination microscopy imaging on mouse PACs and observed high levels of colocalization between TRPV6 and STIM1 in PACs following TG stimulation (Figure 5*C–D*). Coimmunoprecipitation (Co-IP) experiments showed the interaction between TRPV6 and STIM1, and this interaction was increased after TG treatment (Figure 5*E–F*). Furthermore, overexpressing STIM1 in HEK293T cells increased TRPV6-mediated currents (Figure 5*G–H*). These data demonstrate that the physical interactions between STIM1 and TRPV6, at least partly, mediate SOCE-evoked Ca^{2+} currents, which indicate the potential role of TRPV6 in AP pathology via SOCE mechanism.

Pharmacological and Genetic Inhibition of TRPV6 Protects Experimental AP

To explore the therapeutic potential of pharmacological TRPV6 inhibition in AP, we administered varying doses of

Figure 3. (***See previous page***). **TRPV6 inhibition reduces Ca^{2+} influx and cell injury in PACs.** (*A and B*) Live-cell images (*A*) and traces and peak quantification (*B*) of Ca^{2+} fluorescence of PACs incubated with HEPES or SORC27 (100 nM) before and after CCK (100 nM) stimulation (n = 35, 64 cells pooled from 3 independent experiments). (*C and D*) Live-cell images (*C*) and traces and peak quantification (*D*) of Ca^{2+} fluorescence from human PACs incubated with HEPES or SORC27 (100 nM) before and after TLCS (500 μM) stimulation (n = 43, 62 cells pooled from 3 patients with AP). (*E*) Schematic diagram of AAV-si*Trpv6* and AAV-siNC administration to generate conditional knockdown mice. (*F*) Representative images and quantification of *Trpv6* expression in transfected pancreata from siNC and si*Trpv6* mice (n = 8–12 mice per group). (*G*) Live-cell images, traces, and peak quantification Ca^{2+} fluorescence from PACs isolated from either siNC or si*Trpv6* mice prior to and following CCK stimulation (n = 232, 256 cells pooled from 3 independent experiments). (*H*) Representative images and cell death quantification of PACs isolated from either siNC or si*Trpv6* mice at baseline and following CCK (500 nM) or TLCS (500 μM) treatments (n = 4–7 samples pooled from 3 independent experiments). (*I*) Representative live-cell imaging and trace and peak quantification TMRM dye fluorescence intensity from PACs isolated from siNC or si*Trpv6* mice during 15 minutes of CCK (100 nM) exposure (n = 22, 32 cells pooled from 3 independent experiments). (*J*) Representative images of BZiPAR fluorescence obtained by live-cell imaging and trace and peak quantification examining the effect of CCK (100 nM) treatment in PACs isolated from siNC or si*Trpv6* mice (n = 6, 18 cells pooled from 3 independent experiments). Data are the mean ± SEM; $^{*}P < .05$, $^{**}P < .01$, $^{***}P < .001$.

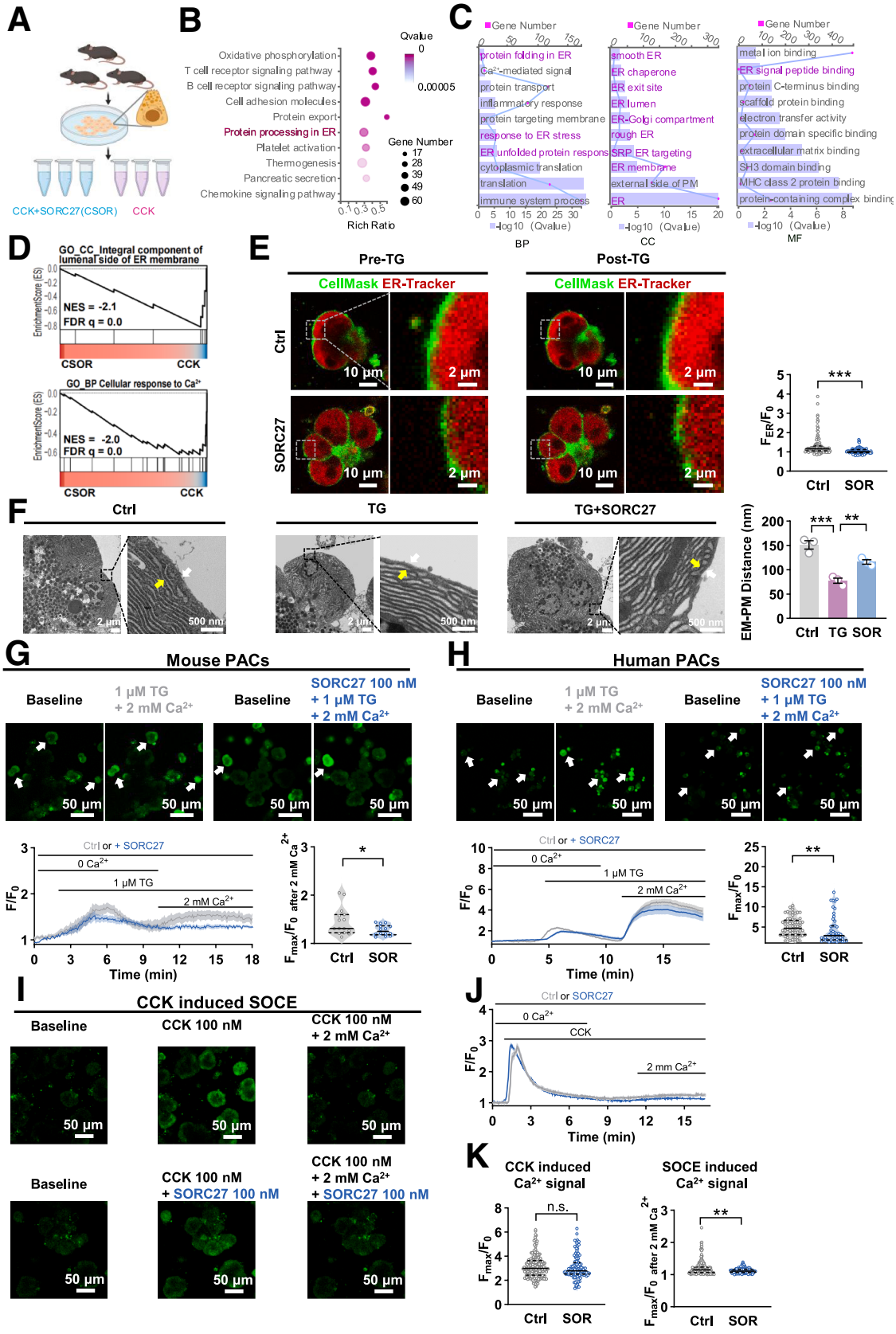
A
CCK+SORC27(CSOR)
CCK
B
Oxidative phosphorylation
T cell receptor signaling pathway
B cell receptor signaling pathway
Cell adhesion molecules
Protein export
Protein processing in ER
Platelet activation
Thermogenesis
Pancreatic secretion
Chemokine signaling pathway
Qvalue
0
0.00005
Gene Number
17
28
39
49
60
Rich Ratio
C
Gene Number
protein folding in ER
Ca2+-mediated signal
protein transport
inflammatory response
protein targeting membrane
response to ER stress
ER unfolded protein respons
cytoplasmic translation
translation
immune system process
-log10 (Qvalue)
BP
smooth ER
ER chaperone
ER exit site
ER lumen
ER-Golgi compartment
rough ER
SRP, ER targeting
ER membrane
external side of PM
ER
CC
metal ion binding
ER signal peptide binding
protein C-terminus binding
scaffold protein binding
electron transfer activity
protein domain specific binding
extracellular matrix binding
SH3 domain binding
MHC class 2 protein binding
protein-containing complex binding
MF
D
GO_CC_Integral component of lumenal side of ER membrane
NES = -2.1
FDR q = 0.0
CSOR
CCK
GO_BP Cellular response to Ca2+
NES = -2.0
FDR q = 0.0
E
Pre-TG
Post-TG
CellMask ER-Tracker
Ctrl
SORC27
10 μm
2 μm
FER/F0
***
Ctrl SOR
F
Ctrl
TG
TG+SORC27
2 μm
500 nm
EM-PM Distance (nm)
***
**
Ctrl TG SOR
G
Mouse PACs
Baseline
1 μM TG
+ 2 mM Ca2+
SORC27 100 nM
+ 1 μM TG
+ 2 mM Ca2+
50 μm
Ctrl or + SORC27
0 Ca2+
1 μM TG
2 mM Ca2+
F/F0
Time (min)
Fmax/F0 after 2 mM Ca2+
*
Ctrl SOR
H
Human PACs
Baseline
1 μM TG
+ 2 mM Ca2+
SORC27 100 nM
+ 1 μM TG
+ 2 mM Ca2+
50 μm
Ctrl or + SORC27
0 Ca2+
1 μM TG
2 mM Ca2+
F/F0
Time (min)
Fmax/F0
**
Ctrl SOR
I
CCK induced SOCE
Baseline
CCK 100 nM
CCK 100 nM
+ 2 mM Ca2+
50 μm
Baseline
CCK 100 nM
+ SORC27 100 nM
CCK 100 nM
+ 2 mM Ca2+
+ SORC27 100 nM
J
Ctrl or SORC27
0 Ca2+
CCK
2 mm Ca2+
F/F0
Time (min)
K
CCK induced
Ca2+ signal
n.s.
Fmax/F0
Ctrl SOR
SOCE induced
Ca2+ signal
**
Fmax/F0 after 2 mM Ca2+
Ctrl SOR

SORC27 intravenously to mice with AP or without modeling for negative controls (Figure 6*A*). Although SORC27 did not affect pancreatic or systematic indexes of normal mice (Figure 6*B* for pain behavior; Figure 6*C* for serum amylase, pancreatic myeloperoxidase [MPO], and trypsin activity; Figure 6*D–E* for histological score), in the case of AP, both low (400 mg/kg) and high (800 mg/kg) doses of SORC27 treatment resulted in increased pain tolerance (Figure 6*F*), decreased serum amylase and pancreatic trypsin activity, and decreased pancreatic MPO without achieving significance (Figure 6*G*). The high dose SORC27 also diminished pancreatic tissue damage by significantly alleviating edema and inflammation (Figure 6*H*), Macrophage recruitment is one of the most important immune responses that exacerbates AP.[3] We found that treatment with SORC27 significantly reduced pancreatic (Figure 6*I*) and lung (Figure 6*J*) macrophage recruitment levels and prevented tissue damage to lungs (Figure 6*K*). Although high-dose SORC27 treatment showed no effect on the level of STIM1 protein (Figure 6*L*), it significantly decreased pancreatic *Stim1* mRNA expression level (Figure 6*M*).

Next, we examined whether pancreatic genetical knockdown of *Trpv6* could similarly rescue various AP-associated phenotypes (Figure 7*A*). Although pancreatic *Trpv6* knockdown (Figure 7*B*) did not affect the parameters in healthy mice (Figure 7*C* for pain behavior; Figure 7*D* for serum amylase, pancreatic MPO, and trypsin activity; Figure 7*E–F* for histological score), during AP, pancreatic si*Trpv6* showed evident beneficial effects including increased pain tolerance (Figure 7*G*), decreased levels of serum amylase, pancreatic MPO, and trypsin activation (Figure 7*H*), and overall decreased pancreatic tissue damage, including reduced levels immune cell infiltration and necrosis significantly (Figure 7*I–J*) compared with siNC mice. Similarly, si*Trpv6* AP mice also had decreased pancreatic (Figure 7*K*) and lung (Figure 7*L*) macrophage infiltration, as well as decreased lung tissue damage (Figure 7*M*) induced by CER injections. Additionally, pancreatic STIM1 was reduced in si*Trpv6* AP mice compared with siNC mice (Figure 7*N–O*). Taken together, these data indicate that blocking TRPV6 ameliorates CER-induced AP in mice, likely through the suppression of STIM1-TRPV6-mediated SOCE.

Discussion

Here, we describe the novel finding that TRPV6 is functionally expressed in human and mouse PACs and interacts with STIM1 to promote both the induction and the maintenance of SOCE during AP. Either pharmacological or genetic approach resulted in reduced TRPV6 function, which could ameliorate disease severity of AP. Together, our data supports TRPV6 as a novel target for AP therapy aimed at reducing Ca^{2+} overload.

Here, we present evidence of increased TRPV6 expression in both mouse and human pancreatic tissues, together with heightened channel activity. The increase of TRPV6 in AP signifies a strong correlation between channel function and disease pathology, and we subsequently validated the beneficial impact of TRPV6 inhibition in AP. The effect of inhibiting TRPV6 on the prevention of cell death in mice PACs might be attributed to the negative modulation of Ca^{2+}-dependent mitochondrial dysfunction and trypsin activation. These two features represent the first-line cellular pathology during AP and significantly contribute to cell death. Notably, both mitochondrial dysfunction and trypsin preactivation are closely related to sustained Ca^{2+} influx in PACs.[61] High Ca^{2+} concentrations promote mitochondrial permeability by transitioning pores to open and high-conductance states, resulting in depolarization and the loss of membrane potential.[8] Meanwhile, SOCE-mediated Ca^{2+} overload was reported to promote trypsin activity by regulating calcineurin and the nuclear factor of activated T cells.[48,62] Nonetheless, more investigation is required to elucidate the importance of TRPV6 increased expression, which may also be attributed to the compensation mechanism of the auto-inhibition nature of TRPV6, given the sophisticated mechanism of the activation gating and channel opening, which appears to be more closely associated with the channel's conformational ensemble.

A recent study,[63] which performed pancreatic single-cell and bulk RNA sequencing in AP mice, revealed the significance of ER-related dysfunction in PACs. Correspondingly, in the current study, the whole transcriptome analyses provide strong evidence for the role of TRPV6 in regulating ER function. This observation led us to the interconnection between SOCE and TRPV6, due to the well-known primary

Figure 4. (***See previous page***). **Pharmacological TRPV6 inhibition affects ER-related cell functions.** (*A*) RNA-seq was performed on freshly isolated PACs treated with 100 nM CCK (CCK) or CCK and 100 nM SORC27 (CSOR) (n = 3 samples from 3 mice per group). (*B*) Top 10 enriched KEGG pathways in CCK-treated PACs in (*A*) with or without SORC27. (*C*) Top 10 GO terms enriched in PACs in (*A*) treated with CCK resulting from the analysis of DEGs in the BP, CC, and MF categories. (*D*) GSEA for the indicated gene sets and the resulting normalized enrichment score (NES) and FDR q values indicated pathways enriched in PACs in (*A*) treated with CCK. (*E*) Live cell images of ER tracker (*red*) and cell mask (*green*) pre- and post-TG (1 μM) in HEPES control (Ctrl) and SORC27 (100 nM) -treated PACs. The relevant intensity changes of ER signal colocalized on the cell membrane were quantified (fluorescent signals were analyzed in the region in the dotted-line box, n = 119, 102 cells pooled from 3 independent experiments). (*F*) Representative images and quantification of EM-PM distance obtained by transmission electron microscopy showing EM-PM junctions in PACs with the indicated treatments (*white arrows* represent the PM, *yellow arrows* represent the EM). (*G*) Live-cell images, traces, and peak quantification of Ca^{2+} fluorescence of mouse PACs treated with HEPES or SORC27 following TG stimulation (n = 15, 14 cells pooled from 3 independent experiments). (*H*) Live-cell images, traces, and peak quantification of Ca^{2+} fluorescence of human PACs treated with HEPES or SORC27 after TG stimulation (n = 64, 49 cells pooled from 3 patients with AP). (*I–K*) Live-cell images (*I*), traces (*J*), and peak quantification (*K*) of of Ca^{2+} fluorescence of mouse PACs treated with HEPES or SORC27 after CCK stimulation (n = 196, 115 cells pooled from 3 mice). Data are the mean ± SEM; *$P < .05$, **$P < .01$, ***$P < .001$.

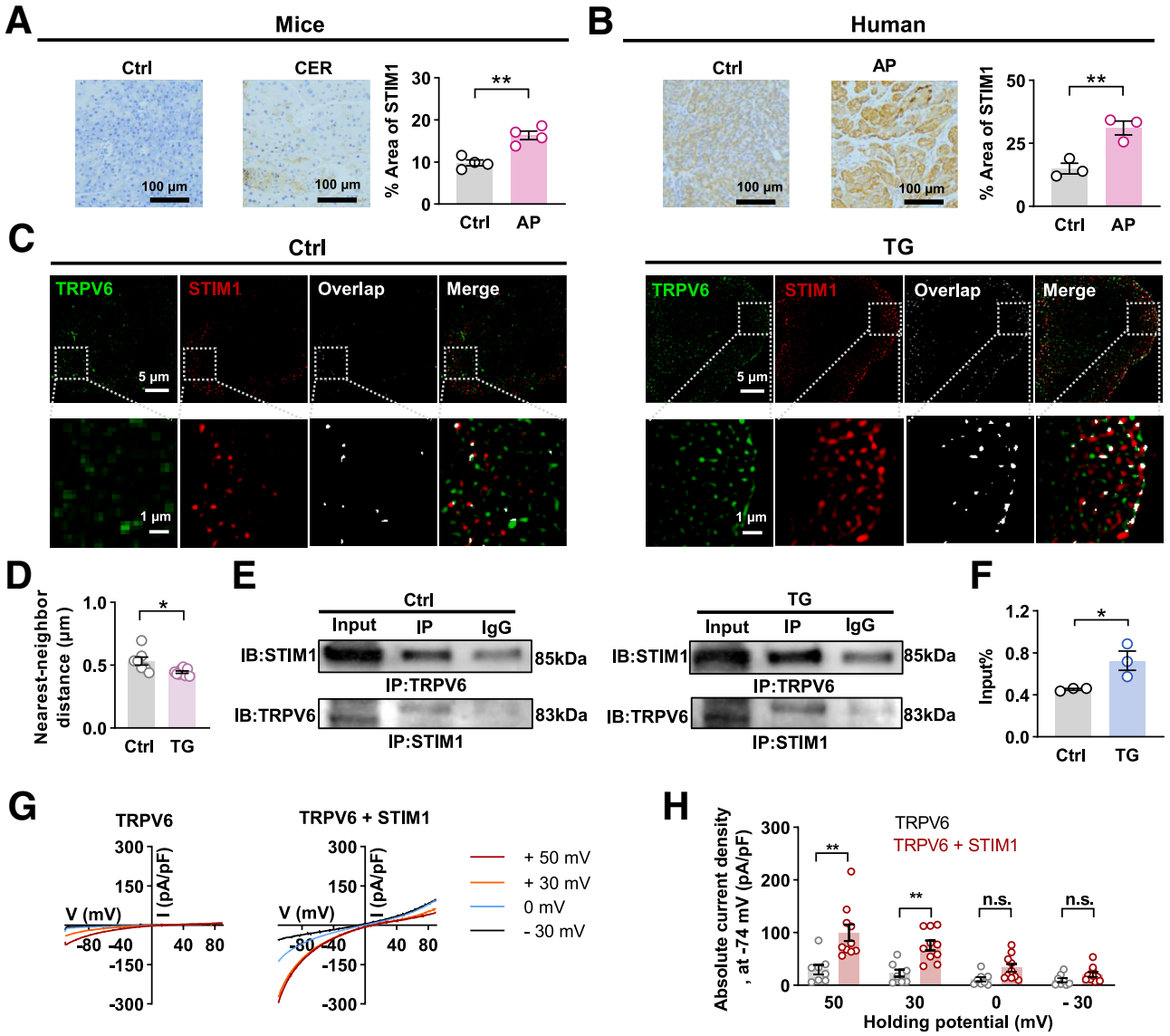

Figure 5. TRPV6 and STIM1 interact in PACs. (*A*) Representative IHC staining images and quantification of STIM1 staining performed on mouse pancreas tissue (n = 4 sections from 3 mice per group). (*B*) Representative IHC staining images and quantification of STIM1 performed on human pancreas tissue (n = 3 sections from 3 patients per group). (*C and D*) Representative images (*C*) and quantification (*D*) of TRPV6 and STIM1 colocalization in PACs obtained by structured illumination microscopy (n = 7–8 regions of interest [ROIs] from 3 independent experiments per group). (*E and F*) Blots (*E*) and quantification (*F*) of Co-IP experiments performed by immunoprecipitating TRPV6 or STIM1 in freshly isolated PAC lysates (n = 3 blots from 3 independent experiments per group). (*G and H*) Representative whole-cell TRPV6 current traces (*G*) and quantification (*H*) of current density at −74 mV under different holding potentials in TRPV6- and STIM1-transfected HEK293T cells (n = 8–10 cells from 4 independent experiments per group). Data are the mean ± SEM; n.s., non-significance, $^{*}P < .05$, $^{**}P < .01$.

function to mediate SOCE of ER in AP pathology.[9,29] The EM-PM junction is composed of membrane contact sites formed between closely approximated EM and PM membranes, which provides a direct route for Ca^{2+} from the extracellular environment to enter the ER, and mediates SOCE.[64] Inhibiting TRPV6 significantly reduced ER translocation towards the PM upon stress, which were observed using live-cell imaging and transmission electron microscopy. A previous study reported that SOCE occurs in PACs near the apical region, where contains high levels of IP_3 receptors.[65] However, our data revealed that the formation of the EM-PM junction occurred in the basal region of PACs. These results agree with other previous work, which found the location of Ca^{2+} entry during SOCE is the basal PACs PM,[66] as well as the observation that STIM1 translocated exclusively to lateral and basal regions of PACs following ER Ca^{2+} store depletion.[60] Together with the SOCE-related Ca^{2+} imaging data in mouse and human PACs, our results provide evidence that TRPV6, at least partly, participates in SOCE in the basal area.

Another important feature for SOCE is the interaction between Ca^{2+} channels and ER Ca^{2+}-senser STIM1. In

human prostate adenocarcinoma cells, inhibiting TRPV6 resulted in decreased Ca^{2+} influx following ER store depletion, which signals SOCE.[39] However, this study failed to witness the physical interaction between TRPV6 and STIM1. On the contrary, we used Co-IP to show that TRPV6 interacts with STIM1 protein in cell lysates from freshly

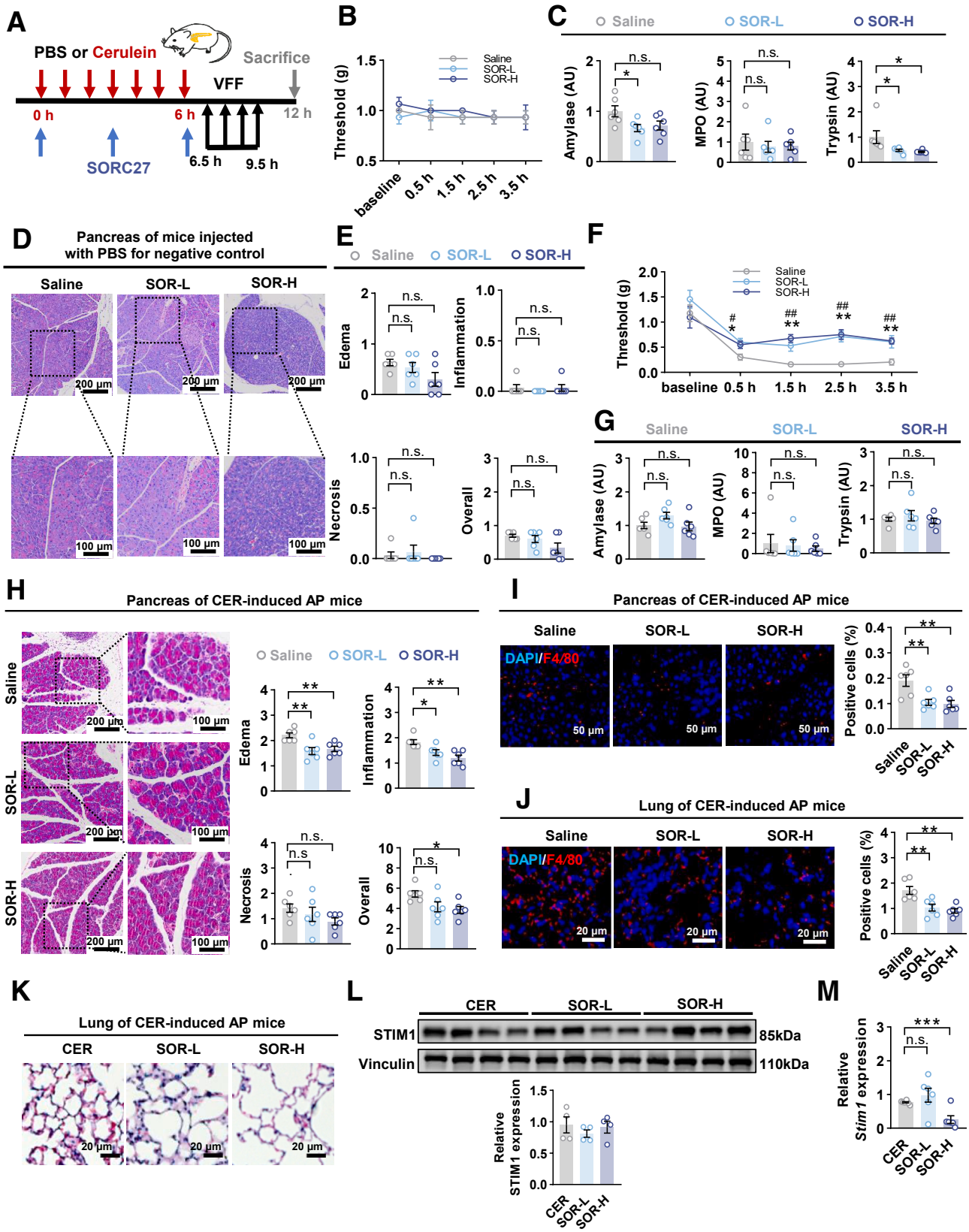

isolated mice PACs, and the interaction was strengthened following TG stimulation. This result was supported by the colocalization of STIM1 and TRPV6 observed using structured illumination microscopy imaging. We next examined the functional consequence of TRPV6 and STIM1 interaction in HEK293T cells; it was found that coexpression of STIM1 and TRPV6 resulted in significantly greater TRPV6-mediated inward rectifying currents, compared with solely TRPV6 expression. Taken together, these results establish a model that, in PACs, following ER Ca^{2+} storage depletion, the ER translocated towards the PM to form the EM-PM junction, STIM1 interacting with TRPV6 to facilitate the opening of the channel, which acts as a source for ER replenishing. Although it remains conflicting that TRPV6 mediates SOCE in multiple cell types, our study provides evidence that in PACs, TRPV6 participates in ER-clearance-induced Ca^{2+} influx and EM-PM junctions, which indicates the involvement of this channel in SOCE mechanism.

Although additional significant SOCE proteins exist on PACs, Orai1 possesses the most therapeutic potential in AP therapy.[67] Despite the potential impact of Orai1 on other systems like intestinal bacterial dysbiosis[68] and T cell activation,[69] other SOCE channels should be proposed as novel drug targets. Although it is difficult to define the proportion of participation rate of these SOCE proteins during AP in PACs, here, we proposed TRPV6 as another critical SOCE mediator, as well as a safe inhibitive drug. SORC27 is a protein-based TRPV6 inhibitor, which was inspired by the paralytic peptide soricidin, a naturally occurring peptide identified in the saliva of the northern short-tailed shrew.[51] Its counterpart, SORC13 (named for its length, 13 amino acids), demonstrated antitumor efficacy in a phase I clinical study with a good safety profile.[70] One limitation of SORC27 is its low potency for inhibiting TRPV6, which was reported by previous studies (inhibiting efficacy of 34%)[51] and in our study (~26%). However, SORC27 could serve as an excellent starting molecule for rational drug design to develop a TRPV6 inhibitor with a more favorable efficacy profile.

It is worth to note that *TRPV6* has been implicated as a novel chronic pancreatitis susceptibility gene by several recent clinical studies that examined nearly 4000 patients from Japan, Germany, France, Poland, and China.[32,71–73] However, mutations were identified in peripheral blood that could potentially be somatic. Additionally, although PACs play an important role in AP, pancreatic stellate cells and ductal cells are more crucial in chronic pancreatitis. How pancreatic TRPV6-mediated calcium disorder affects chronic pancreatitis onset remains unclear. Specific relationships between TRPV6 and the onset of chronic pancreatitis require more investigation. Our results provide a foundation for future research examining Ca^{2+}-dependent chronic pancreatitis initiation mechanisms.

On a separate note, the pancreatic necrosectomy was conducted after at least 4 weeks according to the clinical guideline.[74] Thus, these tissues reflect the late-phase inflammatory injury rather than the early pathology of AP. Although these clinical samples in our study cannot represent the initial inflammation, the TRPV6 expression pattern differed from that of the control group. These findings from clinical samples, at least in part, support our hypothesis regarding TRPV6 and it-mediated Ca^{2+} signals in human pancreatic acinar cells play critical roles during AP.

Conclusions

TRPV6 expression and currents were increased in PACs of AP mice and patients, as well as the presence of TRPV6-mediated SOCE signals, whose mechanism was closely related to the physical interaction between TRPV6 and STIM1. Inhibiting TRPV6 had a protective effect in experimental AP. We offer a new and detailed understanding of how TRPV6 facilitates SOCE in the abnomal Ca^{2+} signaling of AP. This knowledge opens possibilities for developing drugs that specifically target TRPV6 in AP treatment.

Methods

Animal Modeling and Drug Administration

Male C57BL/6J mice (6- to 8-weeks old) were bought from Beijing Huafukang Bioscience Co, Ltd. The animals were housed at 22°C ± 2°C and maintained a 12-hour light-dark cycle. Free access to water and a standard laboratory chow diet were supplied throughout the experiment. The Animal Ethics Committee reviewed and approved all animal experimental procedures (20241014005). To induce AP, mice received 7 intraperitoneal injections of the CCK analog CER (17650-98-5, TOCRIS) (50 μg/kg) at hourly intervals to hyperstimulate the pancreas. Controls received PBS injections at the same volume and frequency. AP

Figure 6. (***See previous page***). **Pharmacological TRPV6 inhibition ameliorates CER-induced AP.** (*A*) Schematic of the in vivo experiments in AP and control mice. (*B*) Line chart displaying the effect of SORC27 on von Frey filament (VFF) test withdrawal thresholds at 0.5, 1.5, 135 2.5, and 3.5 hours following the last PBS injection (n = 6 mice per group). (*C*) Serum amylase, pancreatic MPO, and trypsin activity (n = 6 mice per group). (*D and E*) Representative images (*D*) and histological scores (*E*) of pancreas tissue sections (n = 6 mice per group). (*F*) Line chart displaying the effect of SORC27 on VFF test withdrawal thresholds at 0.5, 1.5, 2.5, and 3.5 hours following the last CER injection (n = 6 mice per group). (*G*) Serum amylase, pancreatic MPO, and trypsin activity (n = 6 samples per group). (*H*) Representative H&E-stained images and histological scores of pancreas tissue sections (n = 6 sections from 6 mice per group). (*I and J*) Representative images of pancreas (*I*) and lung (*J*) tissue section staining for $F4/80^+$ macrophages (*left*) and quantitative results (*right*) (n = 6 sections from 6 mice per group). (*K*) Representative images of lung injury from CER-AP (CER), low (SOR-L) and high (SOR-H) -dose-SORC27 treated mice AP modeling. (*L*) Western blot (WB) images and quantification, and gene expression (*M*) of pancreatic STIM1 after SORC27 treatment (n = 4–6 mice per group). Data are the mean ± SEM; n.s., non-significance, $^*P < .05$, $^{**}P < .01$, $^{***}P < .001$.

severity was analyzed by measuring serum amylase level, pancreatic MPO activity, pancreatic trypsin activity, and histopathology assessments, as described in our previous studies.[75] SORC27 (peptide sequence: EGK LSSND TEGGL CKEFL HPSKV DLPR) was synthesized by Absin Co, Ltd and dissolved in saline before use, 400 mg/kg for low dose or

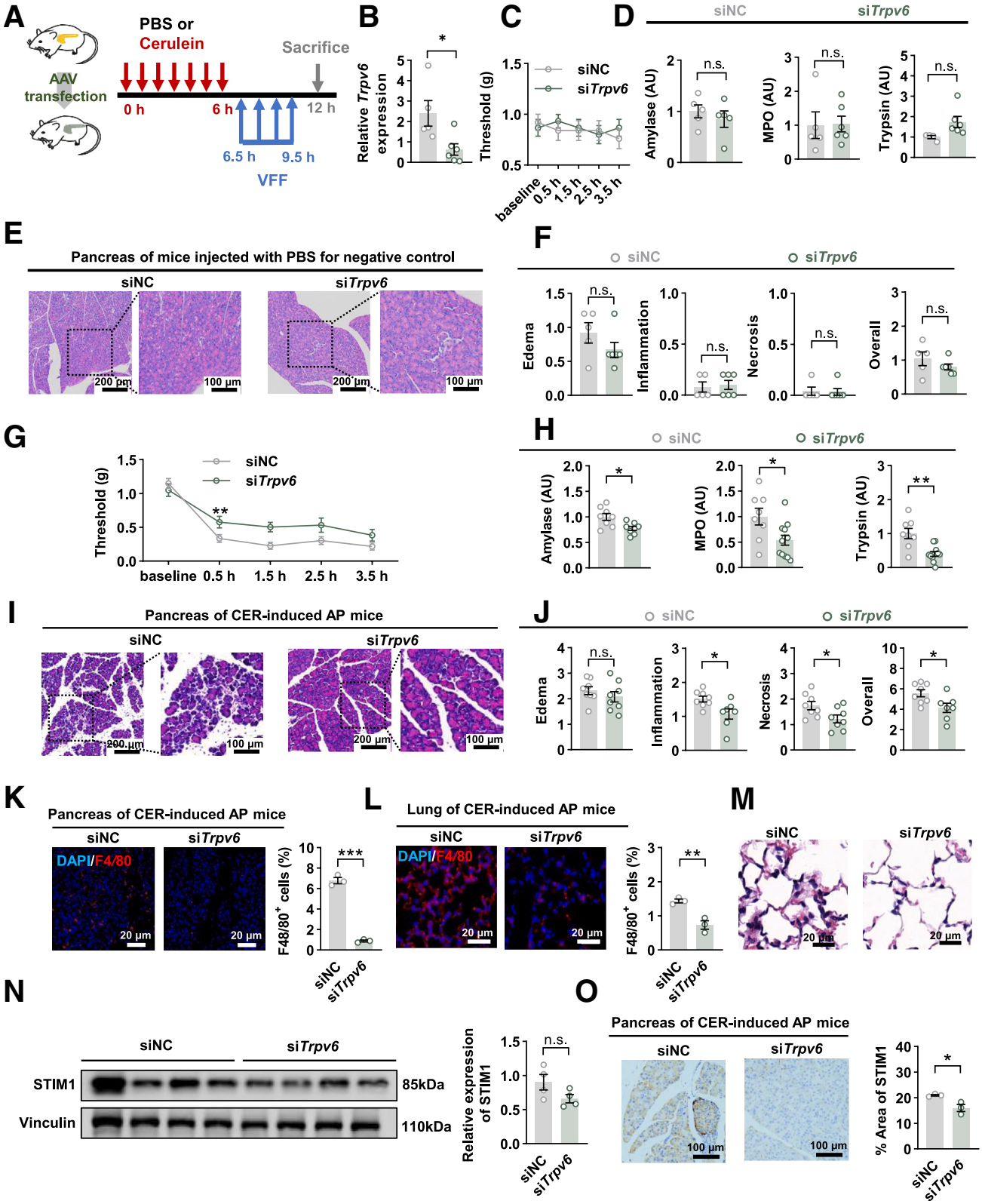

800 mg/kg for high dose. SORC27 was administrated by intravenously in tail vein after the first, fourth, and last CER injection.

Human Sample Collection

Study protocols (2020, No.196) were reviewed and approved by the Institutional Review Board and Biomedical Ethics Committee of West China Hospital, Sichuan University. The biobanking procedures were certified by the China Human Genetic Resources Management Office as a part of West China Biobank (2022, BC0040). Inclusion and exclusion criteria were described previously.[76] Informed consent was obtained from all patients prior to sampling of pancreatic tissues. Samples used as AP group were from adjacent inflammatory pancreatic tissues of resected necrotized tissue during the open necrosectomy procedure; these samples were from the patients who met the criteria for surgical intervention of severe AP. Normal pancreas tissues used as controls were obtained from patients who underwent surgery for left-sided or small unobstructing pancreatic tumors.[77] PACs for electrophysiological measurement and Ca^{2+} imaging were isolated from pancreata of the AP group; tissue sections for RNAscope and immunohistochemical staining were obtained from both Ctrl and AP groups; and main clinical indexes are given in Supplementary Table 1.

In Situ RNAscope and Immunofluorescent Staining

The in situ hybridization assay was performed following our published protocol.[78] The probes and commercial kits were obtained from Advanced Cell Diagnostics. Briefly, paraffinized pancreatic tissue sections (10-μm thickness) were used in a hybridization assay. The specificity of the fluorescent signal of the in situ probes was validated using a negative control probe. After in situ hybridization, slides were blocked with 1% bovine serum albumin (BSA) for 30 minutes and treated with primary antibodies against amylase (sc-46657, Santa Cruz Biotechnology) overnight at 4°C. After incubation with an appropriate secondary antibody and washing, 4',6-diamidino-2-phenylindole (DAPI, 1 g/mL) staining was performed, followed by glycerin sealing and placing a coverslip. Fluorescent images were taken using a confocal microscope (Nikon) and analyzed using ImageJ software (National Institutes of Health).

Isolation of PACs

Freshly isolated PACs from mice were obtained according to our previous procedure.[30] Briefly, mice pancreata were digested in collagenase IV (9001-12-1, Sigma-Aldrich) for 13 minutes, then moved to HEPES buffer (pH 7.3; in mM: HEPES 10, D-glucose 10, NaCl 140, KCl 4.7, $MgCl_2$ 1.13, and $CaCl_2$ 1.2) and pipetted repeatedly. Cells were then filtered with a 70-μm cell strainer. After centrifuge, PACs were resuspended with HEPES buffer. PACs from humans were isolated according to a previous protocol.[79] The surgical specimens of pancreas were transported to the laboratory in Dulbecco's modified Eagle medium (DMEM) on ice within 1 hour after resection. Tissue was injected with collagenase (100 U/mL), minced to 1- to 3-mm diameter, and digested at 37°C with shaking. After 10 minutes, fresh medium was added, followed by mechanical shearing by repeated pipetting and supernatant collection every 15 minutes for 1 hour. Acini were filtered with a 150-μm cell strainer, purified via 4% BSA sedimentation, and suspended in HEPES buffer with 1% BSA and 0.1 mg/mL trypsin inhibitor.

Immunofluorescence

PACs were plated onto an 8-well glass chamber slide (Thermo Fisher), washed with PBS containing 0.1% TWEEN 20, and fixed for 15 minutes using methanol. Following an additional wash, cells were incubated with primary antibodies overnight at 4°C immediately after a blocking step (1 hour with 1% BSA). Then, cells were stained with secondary antibodies for 1 hour at room temperature in the absence of light. After washing, the cells were incubated with DAPI, sealed with glycerin, and covered with coverslip. An A1R+ two-photon confocal scanning microscope (Nikon) was used to capture the fluorescent images.

Electrophysiological Measurements

PACs were plated onto laminin-coated coverslips and used within 6 hours. Whole-cell patch clamp recordings were carried out using an Axon 700B (Molecular Devices). The current signals were filtered at 2 kHz and digitalized at 10 kHz. The pipettes for recording were pulled from borosilicate glass capillaries and had a resistance of 2 to 3 MΩ. The standard extracellular solution contained 145 mM NaCl, 5 mM CsCl, 1 mM $MgCl_2$, 10 mM $CaCl_2$, 10 mM HEPES,

Figure 7. (***See previous page***). **Pancreatic *Trpv6* knockdown alleviates CER-induced AP.** (*A*) Schematic of the in vivo experiments in si*Trpv6* and siNC mice. (*B*) Pancreatic *Trpv6* gene expression (n = 5–6 mice per group). (*C*) Line chart displaying the effect of SORC27 on VFF test withdrawal thresholds at 0.5, 1.5, 2.5, and 3.5 hours following the last PBS injection (n = 6–7 mice per group). (*D*) Serum amylase, pancreatic MPO, and trypsin activity (n = 4–6 mice per group). (*E and F*) Representative images (*E*) and histological scores (*F*) of pancreas tissue sections (n = 5–6 mice per group). (*G*) Line chart indicating VFF withdrawal thresholds observed at 0.5, 1.5, 2.5, and 3.5 hours following the last CER injection (n = 8, 12 mice per group). (*H*) Serum amylase, pancreatic MPO, and trypsin activity (n = 8–12 samples per group). (*I and J*) Representative H&E-stained images (*I*) and histological scores (*J*) of pancreas tissue sections (n = 77–88 sections from at least 8 mice per group). (*K and L*) Representative images and quantitative results of pancreas (*K*) and lung tissue (*L*) $F4/80^+$ staining for macrophages (n = 3 sections from 3 mice per group). (*M*) Representative images of lung injury. (*N*) Immunoblotting images and quantification of STIM1 levels in pancreas tissue (n = 4 samples per group). (*O*) Representative IHC staining images and quantitative results of STIM1 levels in pancreas tissue (n = 3 sections from 3 mice per group). Data are the mean ± SEM; n.s., non-significance, $^*P < .05$, $^{**}P < .01$, $^{***}P < .001$.

and 10 mM glucose (pH 7.4, adjusted with NaOH). The divalent-free (DVF) solution contained 150 mM NaCl, 10 mM HEPES, 10 mM glucose, and 10 mM EGTA (pH 7.4, adjusted with NaOH). The intracellular solution contained 145 mM Cs-methanesulfonate, 8 mM NaCl, 5 mM $MgCl_2$, 10 mM HEPES, and 20 mM EGTA, (pH 7.2, adjusted with CsOH). PACs were clamped at +50 mV. The currents were elicited by 200 ms-voltage ramps from −120 mV to +90 mV every 5 seconds.

Electrophysiological measurements of recombinant TRPV6 channels were performed with HEK293T cells transiently transfected with the cDNA of *TRPV6* and *STIM1* by PolyJet (SL100688, SignaGen Laboratories) according to the manufacturer's instructions. The cells were then cultured with DMEM supplemented with 10% fetal bovine serum (FBS). Electrophysiological recordings were performed 16 hours after transfection. Whole-cell recordings were performed with a patch-clamp amplifier (Axon 700B), and the current signals were filtered at 2 kHz and digitalized at 10 kHz. The pipettes for recording were pulled from borosilicate glass capillaries (Sutter Instrument) and had a resistance of 3 to 4 MΩ. The solutions for recording were the same as those used for studying acutely dissociated PACs. The cells were clamped at 0 mV, and the currents were evoked by 200 ms-voltage ramps from −120 mV to +90 mV every 5 seconds. The stimulation and data acquisition were controlled by Axon Digidata 1440A (Molecular Devices).

Generating and Injecting AAV

AAV-expressing si*Trpv6* or siNC with eGFP or mCherry sequence were packaged and provided by Shanghai Taitool Bioscience Co, Ltd. AAV was administrated to the pancreas using an intraductal infusion system following a previously established protocol.[55] Briefly, 6- to 8-week-old male mice received retrograde pancreatic ductal injection of AAV at a concentration of 1.2×10^{12} virus genome/mL. Mice were infected with AAV for 28 days before AP model establishment by CER treatment. The efficiency of transfection was assessed by fluorescence microscopy and RT-qPCR analysis.

Calcium Imaging

PACs were seeded on coverslips coated with laminin, loaded with 5 μM Fluo-4 AM (F14201, Invitrogen) for 30 minutes at 37°C, and then washed by HEPES buffer solution. Fluorescence was measured by a 2-photon confocal scanning microscope (Nikon) during illumination at 488 nm. PACs were exposed to 100 nM CCK (C2175, Sigma) or 1 μM TG (T7459, Invitrogen) with or without 100 nM SORC27 in HEPES buffer solution. Responding cells were identified as those with an increase in fluorescence intensity of more than 20% compared with baseline. Data was analyzed with ImageJ (National Institutes of Health). For normalization, all data were subjected to F/F0 ratio, and data used for statistics in the violin plots are the signals acquired at the peak time point.

Cell Death Assays

Mouse PACs were freshly isolated and subjected to cell death evaluation according to our previous publication.[75,78] Briefly, cells were loaded with Hoechst 33342 (50 μg/mL) for staining the nuclei and propidium iodide (PI; 1 μM) for assessing plasma membrane integrity. Images were recorded by an Axio Imager 2 epifluorescence microscope (Zeiss). Cell death was determined as the percentage of PI-positive cells of Hoechst-33342-positive cells.

Mitochondrial Depolarization

Live-cell mitochondrial depolarization was analyzed according to a previously described protocol[26] using the mitochondrial labeling dye tetramethylrhodamine (TMRM) (T668, Invitrogen). PACs were incubated with TMRM (200 nM) in HEPES buffer for 30 minutes. The TMRM dye was washed and excited at 555 nm, and the captured images were analyzed with ImageJ software (National Institutes of Health).

Trypsinogen Activation

PACs were coincubated with the active trypsin enzyme substrate BZiPAR (R6505, Invitrogen) at 10 μM according to an established protocol.[26] Cells were maintained in HEPES buffer with 1 mM Ca^{2+} during imaging. BZiPAR was excited at 488 nm. The captured images were analyzed with ImageJ software (National Institutes of Health).

RNA Sequencing and Bioinformatics

Total RNA was extracted from freshly isolated PACs. Cell pellets were transferred into a grinding tube with 600 μL Buffer RLT Plus for homogenization, then centrifuged at 12,000 × *g* for 3 minutes at room temperature. Supernatants were transferred to an AllPrep DNA spin column and centrifuged at 12,000 × *g* for 30 seconds at room temperature. The solution passing into the collection tube was then taken for RNA purification. The quality of the extracted total RNA samples was examined with a Standard Sensitivity RNA Analysis Kit (15 nt) (DNF-471). RNA was denatured, and mRNA was enriched using oligo (dT)-attached magnetic beads, followed by sample fragmentation to obtain a target insert fragment size of ∼150 bp. Fragments were reverse-transcribed into cDNA. After repairing, a single 'A' nucleotide overhang was added to the 3′ ends of the blunt fragments. Following adaptor ligation, fragments were subjected to PCR amplification. Single-stranded PCR products were then produced via denaturation and circularized, while uncircularized linear DNA molecules were digested. Single-stranded circular DNA molecules were then replicated via rolling cycle amplification, and a DNA nanoball (DNB) containing multiple copies of DNA was generated. DNBs of sufficient quality were then loaded into a patterned nanoarray using a high-intensity DNA nanochip technique and sequenced through combinatorial Probe-Anchor Synthesis. The raw data was filtered with SOAPnuke (v1.6.5), and clean reads were obtained and stored in FASTQ format.

Between-group analysis of DEGs was performed by DEseq2 under the conditions of fold change $\geq$0.25 and adjusted *P* value $\leq$ .05. For enrichment analysis, DEG data were analyzed using GO and KEGG analyses that were conducted with the help of the Dr TOM platform (https://mybgi.bgi.com/tech). GSEA was implemented on the Java GSEA platform[80] with the 'Signal2Noise' metric to generate a ranked list and a 'gene set' permutation type. Gene sets with fold change $\geq$0.25 and adjusted *P* value $\leq$ .05 were considered statistically significant.

ER and Cell Membrane Labeling on Living PACs

PACs were incubated with the ER tracker (E34250, Invitrogen) for 30 minutes at 1 μM and following 1 $\times$ Cellmask (C37608, Invitrogen) for 10 minutes. Cells were maintained in HEPES buffer with 1 mM Ca^{2+} during imaging. The ER tracker was excited at 555 nm; Cellmask was excited at 488 nm. The ER tracker fluorescent signal restricted by Cellmask area was recorded. Pre- and post-TG were recorded in both control and SORC27 treated groups. For normalization, all data were subjected to F/F_0 ratio, and data used for statistics in the violin plots are the signals acquired at the peak time point after TG treatment. The captured images were analyzed with ImageJ software (National Institutes of Health).

Transmission Electron Microscopy

Freshly isolated PACs were prefixed in 2.5% glutaraldehyde (pH = 7.4) at 4°C for 4 hours. The samples were then refixed with 1% osmium tetroxide, dehydrated by acetone, and penetrated using dehydrating agent and Epon-812 embedding agent in a 3:1 ratio. Following embedding, samples were sectioned into ultrathin sections and stained with uranyl acetate for 10 minutes and lead citrate for 2 minutes. Samples were observed and photographed by a JEM-1400FLASH transmission electron microscopy (JEOL). The measurement of the distance between the ER membrane and PM was measured with ImageJ (National Institutes of Health) using images with resolution of 0.0028 pixels per micron.

Immunohistochemistry

Pancreatic sections were deparaffinized, subjected to antigen retrieval using a microwave, and then washed in water prior to blocking with normal goat serum for 10 minutes. Then, slides were incubated for 1 hour at room temperature using a primary antibody of STIM1 dilution of 1:100 (NB110-55300, Novus), and then for another hour with biotinylated secondary antibodies (1:1000). Next, horseradish peroxidase (HRP)-bound tertiary antibodies were applied to recognize the secondary antibodies. The sections were then counterstained with hematoxylin after being developed for 5 minutes followed by staining by the diaminobenzidine tetrahydrochloride substrate.

Super-resolution Imaging

Imaging experiments were performed using an N-SIM structured illumination microscopy (Nikon). Raw SIM images contained 9 images each, which were subsequently reconstructed and processed using NIS-Elements AR Analysis. Cluster analysis was performed using a plugin MosaiclA for spatial pattern and interaction analysis in ImageJ software (National Institutes of Health) according to the manufacturer's instructions.[81,82]

Co-IP

The Co-IP assay was performed according to the kit instructions (17-500, Millipore). Briefly, lysates of PACs were immunoprecipitated in IP buffer containing IP antibody-coupled agarose beads, and protein-protein complexes were later analyzed by Western blot. Antibody for TRPV6 (ACC-036, Alomone labs) and STIM1(4916, Cell Signaling Technology) was used. The labeled protein bands were visualized using a Chemiluminescent Detection System (Bio-Rad).

Western Blot

Equal amounts of protein lysates (10 μL of each sample) were separated on 12% SDS-PAGE gels (80 V, 2.5 hours) and then transferred onto polyvinylidene difluoride membranes. After blocking with 5% skim milk for 1 hour, the membranes were incubated with primary antibody (TRPV6, 1:1,000, STIM1, 1:1,000), vinculin (sc-73614, Santa Cruz Biotechnology) (1:1,000) at 4°C overnight. The samples were then incubated with secondary goat anti-mouse IgG-HRP antibody (1:10,000) or goat anti-rabbit IgG-HRP antibody (1:4,000) for 1 hour at room temperature. Protein bands were visualized and analyzed using a Chemiluminescent Detection System (Bio-Rad).

von Frey Test

Methods to assess pain were consistent with our previously established protocol[75,83] using calibrated von Frey filaments (Ugo Basile). The withdrawal threshold of each mouse was detected prior to the initiation of the experiment to establish the baseline, then again measured at four consecutive timepoints of 0.5, 1.5, 2.5, and 3.5 hours after the last (seventh) CER injection (representing 6.5, 7.5, 8.5, and 9 hours after the initial induction of AP).

Hematoxylin and Eosin

Hematoxylin and eosin (H&E) staining was performed according to our previous studies.[30,78] Briefly, mouse pancreatic tissues were collected and fixed in 10% formalin for 24 hours, embedded in paraffin, and cut into sections prior to H&E staining. After deparaffinization, hematoxylin staining, differentiation, and eosin staining, dehydrating and mounting were performed.

RT-qPCR

Total RNA was extracted from the tail of the pancreas as previously described.[84,85] Then, 1 μg total RNA was used as input for reverse transcription into cDNA, followed by RT-qPCR. The RT-qPCR reaction conditions were as follows: 1 cycle of 95°C for 5 minutes, followed by 40 cycles of 95°C

for 20 seconds, 60°C for 20 seconds, and 72°C for 20 seconds using a CFX 96 RT-qPCR instrument (Bio-Rad). The results for relative mRNA expression levels were calculated using the $2^{-\triangle\triangle Ct}$ method and were represented as fold change compared with the control group. The primer sequences are as follows:

Stim1

Forward: 5′-GGCGTGGAAATCATCAGAAGT-3′,
Reverse: 5′-TCAGTACAGTCCCTGTCATGG-3′.

Trpv6

Forward: 5′-CACGTCCCTTTGGTGCCTAT-3′,
Reverse: 5′-CTGATGCTTGGTGAGAGCCA-3′.

18s

Forward: 5′-TTGACTCAACACGGGAAACC-3′,
Reverse: 5′- AGACAAATCGCTCCACCAAC-3′.

Statistical Analysis

All data are presented as mean ± standard error of the mean (SEM). Statistical analyses were performed using GraphPad Prism 8.0.1 software. Data from two groups were analyzed using an unpaired two-tailed Student's *t*-test, whereas multiple groups' data were analyzed using 1-way analysis of variance (ANOVA) with Dunnett's multiple comparison tests or nonparametric tests with the Kruskal-Wallis H test. $P < .05$ represents statistical significance.

Supplementary Material

NOTE: To access the supplementary material accompanying this article, visit the full text version at https://doi.org/10.1016/j.jcmgh.2025.101620.

References

1. Mederos MA, Reber HA, Girgis MD. Acute pancreatitis: a review. JAMA 2021;325:382–390.
2. Jaan A, Sarfraz Z, Farooq U, et al. Incidence, implications and predictors of abdominal compartment syndrome in acute pancreatitis: a nationwide analysis. Pancreatology 2024;24:370–377.
3. Lee PJ, Papachristou GI. New insights into acute pancreatitis. Nat Rev Gastroenterol Hepatol 2019; 16:479–496.
4. Barreto SG, Habtezion A, Gukovskaya A, et al. Critical thresholds: key to unlocking the door to the prevention and specific treatments for acute pancreatitis. Gut 2021; 70:194–203.
5. Crockett SD, Wani S, Gardner TB, et al, American Gastroenterological Association Institute Clinical Guidelines Committee. American Gastroenterological Association Institute Guideline on initial management of acute pancreatitis. Gastroenterology 2018;154:1096–1101.
6. Waldron RT, Lugea A, Pandol SJ. Brake adjustment: Ca (2+) entry pathway provides a novel target for acute pancreatitis therapy. Ann Transl Med 2019;7(Suppl 8): S284.
7. Szatmary P, Grammatikopoulos T, Cai W, et al. Acute pancreatitis: diagnosis and treatment. Drugs 2022; 82:1251–1276.
8. Petersen OH, Gerasimenko JV, Gerasimenko OV, et al. The roles of calcium and ATP in the physiology and pathology of the exocrine pancreas. Physiol Rev 2021; 101:1691–1744.
9. Pallagi P, Madacsy T, Varga A, Maleth J. Intracellular Ca (2+) signalling in the pathogenesis of acute pancreatitis: recent advances and translational perspectives. Int J Mol Sci 2020;2:4005.
10. Son A, Ahuja M, Schwartz DM, et al. Ca(2+) influx channel inhibitor SARAF protects mice from acute pancreatitis. Gastroenterology 2019;157:1660–1672.e2.
11. Ahmad M, Narayanasamy S, Ong HL, Ambudkar I. STIM proteins and regulation of SOCE in ER-PM junctions. Biomolecules 2022;12:1152.
12. Waldron RT, Chen Y, Pham H, et al. The Orai Ca(2+) channel inhibitor CM4620 targets both parenchymal and immune cells to reduce inflammation in experimental acute pancreatitis. J Physiol 2019;597:3085–3105.
13. Yelshanskaya MV, Nadezhdin KD, Kurnikova MG, Sobolevsky AI. Structure and function of the calcium-selective TRP channel TRPV6. J Physiol 2021; 599:2673–2697.
14. Moran MM, McAlexander MA, Biro T, Szallasi A. Transient receptor potential channels as therapeutic targets. Nat Rev Drug Discov 2011;10:601–620.
15. Vigna SR, Shahid RA, Liddle RA. Ethanol contributes to neurogenic pancreatitis by activation of TRPV1. FASEB J 2014;28:891–896.
16. Vigna SR, Shahid RA, Nathan JD, et al. Leukotriene B4 mediates inflammation via TRPV1 in duct obstruction-induced pancreatitis in rats. Pancreas 2011;40:708–714.
17. Noble MD, Romac J, Wang Y, et al. Local disruption of the celiac ganglion inhibits substance P release and ameliorates caerulein-induced pancreatitis in rats. Am J Physiol Gastrointest Liver Physiol 2006; 291:G128–G134.
18. Romac JM, McCall SJ, Humphrey JE, et al. Pharmacologic disruption of TRPV1-expressing primary sensory neurons but not genetic deletion of TRPV1 protects mice against pancreatitis. Pancreas 2008;36:394–401.
19. Hutter MM, Wick EC, Day AL, et al. Transient receptor potential vanilloid (TRPV-1) promotes neurogenic inflammation in the pancreas via activation of the neurokinin-1 receptor (NK-1R). Pancreas 2005; 30:260–265.
20. Wick EC, Hoge SG, Grahn SW, et al. Transient receptor potential vanilloid 1, calcitonin gene-related peptide, and substance P mediate nociception in acute pancreatitis. Am J Physiol Gastrointest Liver Physiol 2006; 290:G959–G969.
21. Noble MD, Romac J, Vigna SR, Liddle RA. A pH-sensitive, neurogenic pathway mediates disease severity in a model of post-ERCP pancreatitis. Gut 2008;57:1566–1571.
22. Shahid RA, Vigna SR, Layne AC, et al. Acinar cell production of leukotriene B(4) contributes to development of neurogenic pancreatitis in mice. Cell Mol Gastroenterol Hepatol 2015;1:75–86.

23. Liddle RA. The role of transient receptor potential vanilloid 1 (TRPV1) channels in pancreatitis. Biochim Biophys Acta 2007;1772:869–878.
24. Schwartz ES, Christianson JA, Chen X, et al. Synergistic role of TRPV1 and TRPA1 in pancreatic pain and inflammation. Gastroenterology 2011;140:1283–1291. e1–2.
25. Ceppa E, Cattaruzza F, Lyo V, et al. Transient receptor potential ion channels V4 and A1 contribute to pancreatitis pain in mice. Am J Physiol Gastrointest Liver Physiol 2010;299:G556–G571.
26. Swain SM, Romac JM, Shahid RA, et al. TRPV4 channel opening mediates pressure-induced pancreatitis initiated by Piezo1 activation. J Clin Invest 2020; 130:2527–2541.
27. Kanju P, Chen Y, Lee W, et al. Small molecule dual-inhibitors of TRPV4 and TRPA1 for attenuation of inflammation and pain. Sci Rep 2016;6:26894.
28. Terada Y, Fujimura M, Nishimura S, et al. Roles of Cav3. 2 and TRPA1 channels targeted by hydrogen sulfide in pancreatic nociceptive processing in mice with or without acute pancreatitis. J Neurosci Res 2015; 93:361–369.
29. Kim MS, Lee KP, Yang D, et al. Genetic and pharmacologic inhibition of the Ca2+ influx channel TRPC3 protects secretory epithelia from Ca2+-dependent toxicity. Gastroenterology 2011;140:2107–2115, 2115. e1–4.
30. Du W, Liu G, Shi N, et al. A microRNA checkpoint for Ca (2+) signaling and overload in acute pancreatitis. Mol Ther 2022;30:1754–1774.
31. Fanczal J, Pallagi P, Gorog M, et al. TRPM2-mediated extracellular Ca(2+) entry promotes acinar cell necrosis in biliary acute pancreatitis. J Physiol 2020; 598:1253–1270.
32. Masamune A, Kotani H, Sorgel FL, et al. Variants that affect function of calcium channel TRPV6 are associated with early-onset chronic pancreatitis. Gastroenterology 2020;158:1626–1641.e8.
33. Shah IA, Prasad H, Banerjee S, et al. A novel frameshift mutation in TRPV6 is associated with hereditary pancreatitis. Front Genet 2022;13:1058057.
34. Mesquita G, Haustrate A, Mihalache A, et al. TRPV6 channel is involved in pancreatic ductal adenocarcinoma aggressiveness and resistance to chemotherapeutics. Cancers (Basel) 2023;15:5769.
35. Yue LX, Peng JB, Hediger MA, Clapham DE. CaT1 manifests the pore properties of the calcium-release-activated calcium channel. Nature 2001;410:705–709.
36. Cui J, Bian JS, Kagan A, McDonald TV. CaT1 contributes to the stores-operated calcium current in Jurkat T-lymphocytes. J Biol Chem 2002;277:47175–47183.
37. Vanden Abeele F, Roudbaraki M, Shuba Y, et al. Store-operated Ca current in prostate cancer epithelial cells -: Role of endogenous Ca transporter type 1. J Biol Chem 2003;278:15381–15389.
38. Voets T, Prenen J, Fleig A, et al. CaT1 and the calcium release-activated calcium channel manifest distinct pore properties. J Biol Chem 2001;276:47767–47770.
39. Raphael M, Lehen'kyi V, Vandenberghe M, et al. TRPV6 calcium channel translocates to the plasma membrane via Orai1-mediated mechanism and controls cancer cell survival. Proc Natl Acad Sci U S A 2014;111:E3870–E3879.
40. Haustrate A, Prevarskaya N, Lehen'kyi V. Role of the TRPV channels in the endoplasmic reticulum calcium homeostasis. Cells 2020;9:317.
41. Haustrate A, Shapovalov G, Spriet C, et al. TRPV6 calcium channel targeting by antibodies raised against extracellular epitopes induces prostate cancer cell apoptosis. Cancers (Basel) 2023;15:1825.
42. Parekh AB, Putney JW Jr. Store-operated calcium channels. Physiol Rev 2005;85:757–810.
43. Palm C, Hartmann K, Weber K. Expression and immunolocalization of calcium transport proteins in the canine duodenum, kidney, and pancreas. Anat Rec (Hoboken) 2010;293:770–774.
44. Wissenbach U, Niemeyer BA, Fixemer T, et al. Expression of CaT-like, a novel calcium-selective channel, correlates with the malignancy of prostate cancer. J Biol Chem 2001;276:19461–19468.
45. Hirnet D, Olausson J, Fecher-Trost C, et al. The TRPV6 gene, cDNA and protein. Cell Calcium 2003;33:509–518.
46. Zhuang L, Peng JB, Tou L, et al. Calcium-selective ion channel, CaT1, is apically localized in gastrointestinal tract epithelia and is aberrantly expressed in human malignancies. Lab Invest 2002;82:1755–1764.
47. Gorelick FS, Thrower E. The acinar cell and early pancreatitis responses. Clin Gastroenterol Hepatol 2009;7(11 Suppl):S10–S14.
48. Raraty M, Ward J, Erdemli G, et al. Calcium-dependent enzyme activation and vacuole formation in the apical granular region of pancreatic acinar cells. Proc Natl Acad Sci U S A 2000;97:13126–13131.
49. Perides G, Laukkarinen JM, Vassileva G, Steer ML. Biliary acute pancreatitis in mice is mediated by the G-protein-coupled cell surface bile acid receptor Gpbar1. Gastroenterology 2010;138:715–725.
50. Kumar A, Bhatia M. Role of hydrogen sulfide, substance P and adhesion molecules in acute pancreatitis. Int J Mol Sci 2021;22:12136.
51. Bowen CV, DeBay D, Ewart HS, et al. In vivo detection of human TRPV6-rich tumors with anti-cancer peptides derived from soricidin. PLoS One 2013;8:e58866.
52. Bhardwaj R, Lindinger S, Neuberger A, et al. Inactivation-mimicking block of the epithelial calcium channel TRPV6. Sci Adv 2020;6:eabe1508.
53. Bodding M. Voltage-dependent changes of TRPV6-mediated Ca2+ currents. J Biol Chem 2005; 280:7022–7029.
54. Petersen OH. The 2022 George E. Palade Medal Lecture: toxic Ca(2+) signals in acinar, stellate and endogenous immune cells are important drivers of acute pancreatitis. Pancreatology 2023;23:1–8.
55. Xiao X, Guo P, Prasadan K, et al. Pancreatic cell tracing, lineage tagging and targeted genetic manipulations in multiple cell types using pancreatic ductal infusion of adeno-associated viral vectors and/or cell-tagging dyes. Nat Protoc 2014;9:2719–2724.

56. Lytton J, Westlin M, Hanley MR. Thapsigargin inhibits the sarcoplasmic or endoplasmic reticulum Ca-ATPase family of calcium pumps. J Biol Chem 1991; 266:17067–17071.
57. Son A, Park S, Shin DM, Muallem S. Orai1 and STIM1 in ER/PM junctions: roles in pancreatic cell function and dysfunction. Am J Physiol Cell Physiol 2016; 310:C414–C422.
58. Cohen HA, Zomot E, Nataniel T, et al. The SOAR of STIM1 interacts with plasma membrane lipids to form ER-PM contact sites. Cell Rep 2023;42:112238.
59. Ong HL, Liu X, Tsaneva-Atanasova K, et al. Relocalization of STIM1 for activation of store-operated Ca(2+) entry is determined by the depletion of subplasma membrane endoplasmic reticulum Ca(2+) store. J Biol Chem 2007;282:12176–12185.
60. Lur G, Haynes LP, Prior IA, et al. Ribosome-free terminals of rough ER allow formation of STIM1 puncta and segregation of STIM1 from IP(3) receptors. Curr Biol 2009;19:1648–1653.
61. Gryshchenko O, Gerasimenko JV, Peng S, et al. Calcium signalling in the acinar environment of the exocrine pancreas: physiology and pathophysiology. J Physiol 2018;596:2663–2678.
62. Zhu ZD, Yu T, Liu HJ, et al. SOCE induced calcium overload regulates autophagy in acute pancreatitis via calcineurin activation. Cell Death Dis 2018;9:50.
63. Yang K, Xie R, Xiao G, et al. The integration of single-cell and bulk RNA-seq atlas reveals ERS-mediated acinar cell damage in acute pancreatitis. J Transl Med 2024; 22:346.
64. Venkatachalam K, van Rossum DB, Patterson RL, et al. The cellular and molecular basis of store-operated calcium entry. Nat Cell Biol 2002;4:E263–E272.
65. Hong JH, Li Q, Kim MS, et al. Polarized but differential localization and recruitment of STIM1, Orai1 and TRPC channels in secretory cells. Traffic 2011;12:232–245.
66. Petersen OH, Courjaret R, Machaca K. Ca(2+) tunnelling through the ER lumen as a mechanism for delivering Ca (2+) entering via store-operated Ca(2+) channels to specific target sites. J Physiol 2017;595:2999–3014.
67. Bruen C, Miller J, Wilburn J, et al. Auxora for the treatment of patients with acute pancreatitis and accompanying systemic inflammatory response syndrome: clinical development of a calcium release-activated calcium channel inhibitor. Pancreas 2021;50:537–543.
68. Ahuja M, Schwartz DM, Tandon M, et al. Orai1-mediated antimicrobial secretion from pancreatic acini shapes the gut microbiome and regulates gut innate immunity. Cell Metab 2017;25:635–646.
69. Hogan PG, Lewis RS, Rao A. Molecular basis of calcium signaling in lymphocytes: STIM and ORAI. Annu Rev Immunol 2010;28:491–533.
70. Fu S, Hirte H, Welch S, et al. First-in-human phase I study of SOR-C13, a TRPV6 calcium channel inhibitor, in patients with advanced solid tumors. Invest New Drugs 2017;35:324–333.
71. Zou WB, Wang YC, Ren XL, et al. TRPV6 variants confer susceptibility to chronic pancreatitis in the Chinese population. Hum Mutat 2020;41:1351–1357.
72. Oracz G, Zarod M, Ewers M, et al. Loss of function TRPV6 variants are associated with chronic pancreatitis in nonalcoholic early-onset Polish and German patients. Pancreatology 2021;21:1434–1442.
73. Hamada S, Masson E, Chen JM, et al, GREPAN (Genetic Research on PANcreatitis) Study Group. Functionally deficient TRPV6 variants contribute to hereditary and familial chronic pancreatitis. Hum Mutat 2022;43:228–239.
74. Tenner S, Vege SS, Sheth SG, et al. American College of Gastroenterology Guidelines: management of acute pancreatitis. Am J Gastroenterol 2024;119:419–437.
75. Han C, Du D, Wen Y, et al. Chaiqin chengqi decoction ameliorates acute pancreatitis in mice via inhibition of neuron activation-mediated acinar cell SP/NK1R signaling pathways. J Ethnopharmacol 2021;274:114029.
76. Shi N, Liu T, de la Iglesia-Garcia D, et al. Duration of organ failure impacts mortality in acute pancreatitis. Gut 2020;69:604–605.
77. Murphy JA, Criddle DN, Sherwood M, et al. Direct activation of cytosolic Ca2+ signaling and enzyme secretion by cholecystokinin in human pancreatic acinar cells. Gastroenterology 2008;135:632–641.
78. Rong J, Han C, Huang Y, et al. Inhibition of xanthine oxidase alleviated pancreatic necrosis via HIF-1alpha-regulated LDHA and NLRP3 signaling pathway in acute pancreatitis. Acta Pharm Sin B 2024;14:3591–3604.
79. Ji B, Bi Y, Simeone D, et al. Human pancreatic acinar cells lack functional responses to cholecystokinin and gastrin. Gastroenterology 2001;121:1380–1390.
80. Subramanian A, Tamayo P, Mootha VK, et al. Gene set enrichment analysis: a knowledge-based approach for interpreting genome-wide expression profiles. Proc Natl Acad Sci U S A 2005;102:15545–15550.
81. Shivanandan A, Radenovic A, Sbalzarini IF. MosaicIA: an ImageJ/Fiji plugin for spatial pattern and interaction analysis. BMC Bioinformatics 2013;14:349.
82. van de Linde S. Single-molecule localization microscopy analysis with ImageJ. J Phys D Appl Phys 2019;52.
83. Qiu Y, Huang L, Fu J, et al. TREK channel family activator with a well-defined structure-activation relationship for pain and neurogenic inflammation. J Med Chem 2020;63:3665–3677.
84. Wen Y, Han C, Liu T, et al. Chaiqin chengqi decoction alleviates severity of acute pancreatitis via inhibition of TLR4 and NLRP3 inflammasome: identification of bioactive ingredients via pharmacological sub-network analysis and experimental validation. Phytomedicine 2020;79:153328.
85. Ma X, Jin T, Han C, et al. Aqueous extraction from dachengqi formula granules reduces the severity of mouse acute pancreatitis via inhibition of pancreatic pro-inflammatory signalling pathways. J Ethnopharmacol 2020;257:112861.

Received September 27, 2024. Accepted August 26, 2025.

Correspondence
Address correspondence to: Wei Huang, MD, PhD, Ruotian Jiang, PhD, and Qing Xia, MD, No. 37 Guoxue Alley, Wuhou District, Chengdu, 610041. e-mail: dr_wei_huang@scu.edu.cn; ruotianjiang@scu.edu.cn; xiaqing@medmail.com.cn; tel: +86-28- 85423373.

Acknowledgments
The authors thank Xiaoting Chen (Experimental Animal Center) for the technical support in preparing the AAV-induced si*Trpv6* mice, Chunjuan Bao and Fei Chen (Institute of Clinical Pathology) for the technical assistance with H&E staining, Yun Ma and Yang Luo (West China Biobank) for the human sample collection, Rui Wang and Wanmeng Li (Mass Spectrometry Center) for helping with RNA seq analysis, Qiuxiao Shi and Yaping Wu (Histology and Imaging Platform) for helping with the structured illumination microscopy imaging and analysis. All the staff and facilities are from West China Hospital of Sichuan University.

CRediT Authorship Contributions
Chenxia Han (Formal analysis: Lead; Investigation: Lead; Writing – original draft: Lead)
Yuncheng Luo (Formal analysis: Lead; Investigation: Lead)
Zhenlu Li (Resources: Lead)
Lu Li (Investigation: Lead)
Jiawang Li (Investigation: Lead)
Ping Liao (Methodology: Lead)
Li Li (Methodology: Equal)
Juan Lin (Investigation: Supporting)
Shiyu Liu (Investigation: Supporting)
Tingting Liu (Methodology: Supporting)
Dan Du (Methodology: Supporting)
Wei Huang (Supervision: Equal)
Ruotian Jiang (Conceptualization: Lead; Writing – review & editing: Lead)
Qing Xia (Conceptualization: Lead; Funding acquisition: Lead; Supervision: Lead; Writing – review & editing: Equal)

Conflicts of interest
The authors disclose no conflicts.

Funding
The study was supported by the National Natural Science Foundation of China (No. 82104598 to Chenxia Han, No. 82271249 to Ruotian Jiang, No. 82274321 to Qing Xia, No. 82270672 to Wei Huang), 1-3-5 Project for Disciplines of Excellence of West China Hospital, Sichuan University (ZYJC21034, and ZYYC23002 to Ruotian Jiang), Project of Sichuan Provincial Administration of Traditional Chinese Medicine (No. 2023ZD04 to Qing Xia), and Key Research and Development Project of Sichuan Province (No. 2024YFFK0153 to Chenxia Han).

Data Availability
Supplementary data are provided with this paper. All data are also available upon request.